GIAN PIERO CELATA (*) - MAURIZIO CUMO (**) - ANDREA MARIANI (*)

High heat Flux Burnout in Subcooled Flow Boiling: Experimentation and Modelling

Abstract - The paper reports the results of an experimental research carried out at the Heat Transfer Unit of the Energy Department, C.R. Casaccia, on the thermal hydraulic characterization of subcooled flow boiling CHF under typical conditions of thermonuclear fusion reactors, i.e. high liquid velocity and subcooling, together with a theoretical modelling of the phenomenon.

The experiment was carried out exploring the following parameters: channel diameter (from 0.25 to 8.0 mm), heated length (from 1 to 15 cm), liquid velocity (from 2 to 50 m/s), exit pressure (from atmospheric to 5.0 MPa), inlet temperature (from 20 to 80 °C), channel orientation (vertical and horizontal). A maximum CHF value of 60.6 MW/m^2 has been obtained under the following conditions: T_{in} = 30 °C, p = 2.5 MPa, u = 40 m/s, D = 2.5 mm (smooth channel). A higher CHF value can be obtained using capillary tubes (up to 70 MW/m^2).

Turbulence promoters (helically coiled wires) have been employed to further enhance the CHF attainable with subcooled flow boiling. Helically coiled wires allow an increase of 50% of the maximum CHF obtained with smooth channels.

A new model for the prediction of the critical heat flux (CHF) of subcooled flow boiling based on the liquid sublayer dryout mechanism, i.e. the dryout of a thin liquid layer beneath an intermittent vapour blanket due to the coalescence of small bubbles is also presented. The model is focused on the analysis of the CHF in subcooled flow boiling under conditions of very high mass flux and liquid subcooling, typical of fusion reactors thermal hydraulic design, and is characterized by the absence of empirical constants always present in earlier models. Peripheral non-uniform heating and/or twisted-tape inserts are accounted for in the model, originally developed for uniform heating and straight flow. Simultaneous occurring of the two events is also well predicted by the model.

1. Introduction

Among the many technical challenges that fusion technology rose in the recent past, particular interest was reserved to the handling of the plasma and the heat

(*) ENEA Energy Department, Via Anguillarese, 301 I-00060 S.M. Galeria, Rome, Italy.

(**) Univ. dei XL. Cattedra di Impianti Nucleari. Università degli Studi di Roma «La Sapienza».

from fusion reactions. In particular, some components of fusion reactors, such as divertors, plasma limiters, neutral beam calorimeter, ion dumps and first-wall armor, are estimated to be subjected to very high heat loads. Heat fluxes to be removed range from 2 to 40 MW/m², and forced convective subcooled boiling can accommodate these very high heat fluxes. Subcooled flow boiling has been widely investigated in the past [1-3] with particular reference to the thermal hydraulic design of Light Water Reactors (LWR), where the order of magnitude of heat fluxes to be removed was around 1 MW/m². As is well known, this forced convective boiling involves a locally boiling liquid, whose bulk temperature is below the saturation, flowing over a surface exposed to a high heat flux. However, successful use of subcooled flow boiling for high heat fluxes removal requires the critical heat flux (CHF), which is described as a sharp reduction in the energy transfer from a heated surface, not to be reached.

The occurrence of CHF, for the case of heat flux controlled systems, results in a significant increase of the wall temperature, which is usually well above that at which serious damage or "burnout" of the heating surface occurs. A review of recent experiments and predictive aspects of burnout at very high heat fluxes was given by Celata [4]. Macroscopic parameters affecting the CHF condition in subcooled boiling, as given by Collier [2], are subcooling, mass flux, pressure, diameter, and length-to-diameter ratio. In 1984 Boyd [5-6] reported a thorough review of CHF in subcooled flow boiling (with about 300 papers quoted), showing that studied performed in the past were essentially devoted to the thermal hydraulics of LWRs (high pressure, low velocity and low subcooling). Fusion technology requirements gave rise over the last five-six years to a rush in the production of experimental data for subcooled flow boiling CHF in water, under conditions of low-intermediate pressure (up to 5 MPa), high liquid velocity (up to 40 m/s), high liquid subcooling (up to 250 K) and small-intermediate channel diameter (1-15 mm) [7]. Use of turbulence promoters such as twisted tapes or helically coiled wires, was pursued to enhance the thermal performance of subcooled flow boiling [15].

For calculation and design purposes it is also necessary to have reliable predictive tools, such as correlations and models. With regard to correlations, recent papers by Inasaka and Nariai [16], Yin *et al.* [17], and Celata *et al.* [31] showed that few of the existing correlations may provide consistent predictions of water subcooled flow boiling CHF at high heat fluxes. They were originally recommended for operating conditions typical of Pressurized Water Reactor (i.e. CHF an order of magnitude lower than fusion reactors high heat flux components), in relation of which water subcooled flow boiling CHF was extensively studied in the past [2-5].

As is known, models have the advantage, with respect to correlations, to characterize not only the developing data base, but also to be used for the prediction of the CHF beyond the operating conditions of the reference data set.

Unfortunately, a full understanding of the basic mechanisms of subcooled flow boiling CHF at high liquid velocity and subcooling has not been accomplished so far [4]. Consequently, existing models [18, 19, 32], although mechanistic in nature, make use of empirical correlations or parameters deduced from a best-fit procedure through available data sets. Likely to correlations, their use outside the experimental ranges of developing data sets cannot therefore be reliable. Even if the Katto model [32] gives an acceptable prediction of existing data points of CHF at high mass flux and subcooling, its use is nonetheless limited to thermal hydraulic conditions such to provide high exit bulk subcooled conditions (i.e. almost 51% of existing data points) [31].

The aim of the present paper is to report the results of an experimental activity carried out, and still in progress, at the Heat Transfer Unit of the Energy Department of ENEA (CR Casaccia), devoted to the investigation of fundamental aspects of the CHF in subcooled flow boiling at very high heat fluxes [7], together with the proposal of a new mechanistic model for the prediction of water subcooled flow boiling CHF. Although the proposed model is specifically thought for high heat flux applications, it is nonetheless valid for general conditions of the CHF in subcooled flow boiling.

2. Experimental apparatus and test section

The schematic diagram of the employed water loop is drawn in Fig. 1. The loop is made of Type 304 stainless steel and filled with tap water passed through deionizing particulate beds (not shown in the figure).

The mass flow rate is elaborated by two different pumps. The high mass flow rate is obtained using an alternative pump (a three-head piston pump), the maximum volumetric flow rate of which is 2000 l/h. It is connected to a damper to further reduce pressure oscillations while maintaining stable flow conditions (residual pulsation below 2.5%).

The low mass flow rate is obtained using a pump of the eccentric type, characterized by a maximum volumetric flow rate of 80 l/h. Four turbine flow meters (maximum error 0.5%) with different ranges are installed to measure the water flow rate. The ranges are 2.5-25 l/h, 10-100 l/h, 50-500 l/h and 50-500 l/h respectively.

The test section is generally vertically oriented with water flowing upwards. Test sections (one for each run) are made of Type 304 stainless steel (electric resistivity at 500 K is 93 μΩcm), uniformly heated by Joule effect using a 200-kW (50 V and 4000 A, dc) electric feeder. After each test the test section is changed because of the destructive burnout occurrence. Of course not all the electrical power is available for the test section, as it depends from the electrical resistance of this latter, which is a function of the diameter and of the temperature (through the

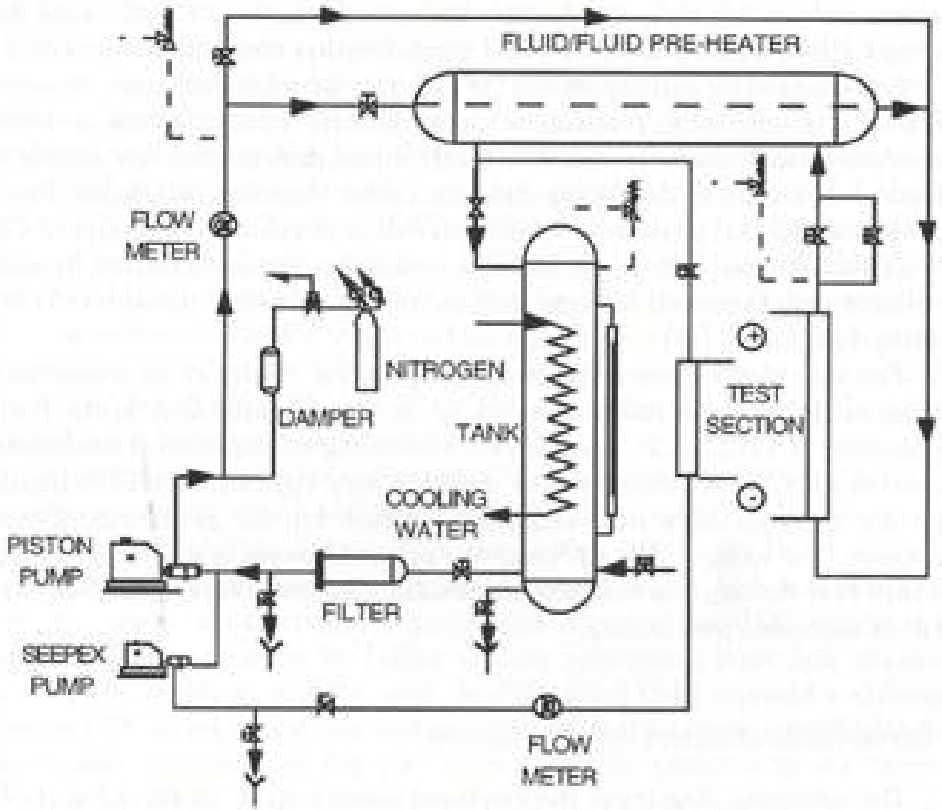

Fig. 1. Schematic of the experimental apparatus.

electrical resistivity). Eleven different test section inner diameters were used. In addition to the heated length of 0.1 m, for the test section D = 8.0 mm, some tests were carried out with a heated length of 0.15 m, and, among these, some were performed with the test section placed in the horizontal position. For the D = 8.0 mm, L = 0.1 m test section, tests were carried out with the insertion of helically coiled wires inside the tube as turbulence promoters. Wires are of spring steel, and their presence does not appreciably affect the electrical resistance of the tube. The test section is connected to copper feed clamps, by means of which it is possible to transfer the electric current to the tube. The power was computed by evaluating the product of the voltage drop across the test section and the current flowing through the walls of the test section. The current was computed from the measurement of the voltage drop (in millivolts) across a precision shunt resistor. Thermal expansion of the test section is mechanically allowed (up to 1.5 mm), thus preventing the rupture of the tube due to thermally induced compressive stresses. Before entering the test section, the water flows through an unheated tube, of the same diameter as the test section, to assure that the liquid velocity profile is fully

developed. The unheated tube length is twice the entrance length, L_u, calculated, under the most severe conditions (highest value of Reynolds number), using:

$$\frac{L_u}{D} = 0.008\ Re^{0.683} \tag{1}$$

Pressure taps are placed just upstream of the unheated length inlet and just downstream of the heated length exit. The static pressure is measured by unsealed strain-gauge absolute pressure transducers (maximum error 0.5%). It is therefore possible to evaluate the pressure gradient in the test channel once the hydraulic characteristics under no-power conditions are known. The pressure at the exit of the test channel is regulated by an electrically controlled valve. The bulk fluid temperature is measured just upstream, T_{Lin}, and downstream, T_{Lout}, this latter, after a suitable mixing of the liquid (obtained with a cross mixer to get the temperature profile flat), of the test section using 0.5 mm K-type thermocouples placed at the center of the channel. Also, all the possible bubbles present are collapsed. The knowledge of T_{Lin} and T_{Lout}, together with the measurement of the water mass flow rate, allows the computation of the thermal power delivered to the fluid by the heat balance in the coolant (calorimetric method). In fact, in all the tests performed (even at burnout conditions), the outlet bulk fluid temperature measurements always revealed the subcooling conditions of the water bulk at the test section exit. In this way heat loss from the test section are bypassed. The employed test sections are not instrumented with wall thermocouples.

Downstream of the test section, the fluid passes through the fluid-to-fluid pre-heater and then in the water cooled tank, where the fluid is cooled down to 25 °C even at the maximum thermal power delivered to the fluid, closing the loop through the filter, towards the piston pump. The maximum pressure of the loop is 7.0 MPa, while the maximum operating temperature of the pump is 70 °C. The fluid-to-fluid pre-heater allows to carry out experiments with a water inlet temperature above 70 °C.

3. Experimental procedure

All the parameters are continuously monitored using digital and analog displays, and each variation is recorded. The experimental procedure consists in the following actions. First, the mass flow rate is set up using the manual control of the piston pump. Secondly, the exit pressure is established using the exit control valve. Once flow rate and exit pressure are steady, thermal power is added to the test section. The control parameter used while approaching the CHF is the electrical power delivered to the walls of the test section, and the initial increment in thermal power is 0.5 kW. Once 70% of the expected CHF value, obtained using

the Gunther correlation [20] which is very simple and gives a conservative prediction of the CHF (SI units):

$$q''_{crit} = 71987\, u^{0.5}\, \Delta T_{Sub} \qquad (2)$$

is reached, the increment is reduced to 0.1 kW (0.1-0.6% of the CHF). After each increment, small adjustments are made in both the exit pressure and flow rate, so that the exit flow conditions correspond to the desired ones. The above reported procedure is repeated until burnout occurs, evidenced by test section destruction and detected by the sharp drop in the electrical power. Video movies show the existence, at burnout, of a narrow glowing area uniformly distributed around the perimeter, and located within 5.0 mm from the top copper feed clamp. A computerized data acquisition system records the measured parameters at the occurring of burnout.

4. Experimental results

The aim of the present research was to characterize the CHF in subcooled flow boiling of water in smooth channels, in order to establish the bounds of the thermal hydraulic design of high heat flux components in fusion reactors. The effect of helically coiled wires as turbulence promoters for the enhancement of the CHF was also studied [7]. Experiments were carried out in channels of 2.5 mm, 4.0 mm, 5.0 mm, 6.0 mm and 8.0 mm [7], together with a specific research devoted to capillary tubes, testing channel diameters from 0.25 mm to 1.7 mm [21]. Effect of channel heated length and channel orientation (horizontal against vertical) was also investigated [7], together with the effect of the tube wall thickness [21].

Test conditions, for a total of 367 points, were selected by the combination of the following parameters:

— tube inside diameter, D:	0.25, 0.5, 0.7, 1.2, 1.5, 1.7, 2.5, 4.0, 5.0, 6.0 and 8.0 mm (± 0.01 mm)
— heated length, L:	from 1 cm to 15 cm
— wall thickness, t:	from 0.25 mm to 1.2 mm (± 0.01 mm)
— tube material:	AISI 304 Type
— water mass flux, G:	from 2 to 50 Mg/m²s
— exit pressure, p:	from 0.1 to 5.0 MPa
— water inlet temperature, T_{in}:	from 20 to 81 °C
— orientation of the test section:	vertical and horizontal (only for L = 0.15 m and 8.0 mm)
— wire diameter, d:	0.5, 0.7 and 1.0 mm
— wire pitch, γ:	from 1.5 to 20.0 mm
— wire material:	spring steel

Tests with turbulence promoters were carried out only with the D = 8.0 mm test sections, L = 0.1 m, vertical position.

4.1. *Effect of mass flux*

The influence of mass flux on the CHF is shown in Fig. 2, where the experimental CHF is plotted versus mass flux G, for D = 2.5 mm. The almost linear dependence of the CHF on G is observed for all the diameters tested. In principle, this would allow to increase the CHF just increasing the mass flux: looking at the figure, it is possible to observe that the CHF can be increased up to a factor of about three passing from 12 to 40 Mg/m²s. From a practical viewpoint it is necessary to consider that pressure drop is related to the square of the velocity and therefore mass flux can not be increased without limits because of that and because, also, of induced vibrations. It is, however, interesting to observe that very high values of the CHF can be accommodated, over 60 MW/m², using the subcooled flow boiling regime of heat transfer.

4.2. *Effect of inlet subcooling*

A significant effect on the CHF is exerted by the liquid inlet temperature, i.e. the inlet subcooling, other conditions being equal, of course in the sense that at a lower inlet temperature (higher subcooling) a higher CHF is obtained (see Fig. 2). Referring to the data in Fig. 2, the ratio between the maximum value of the CHF (T_{in} = 30 °C) and the minimum one (T_{in} = 70 °C) ranges from 1.6 (at G = 11

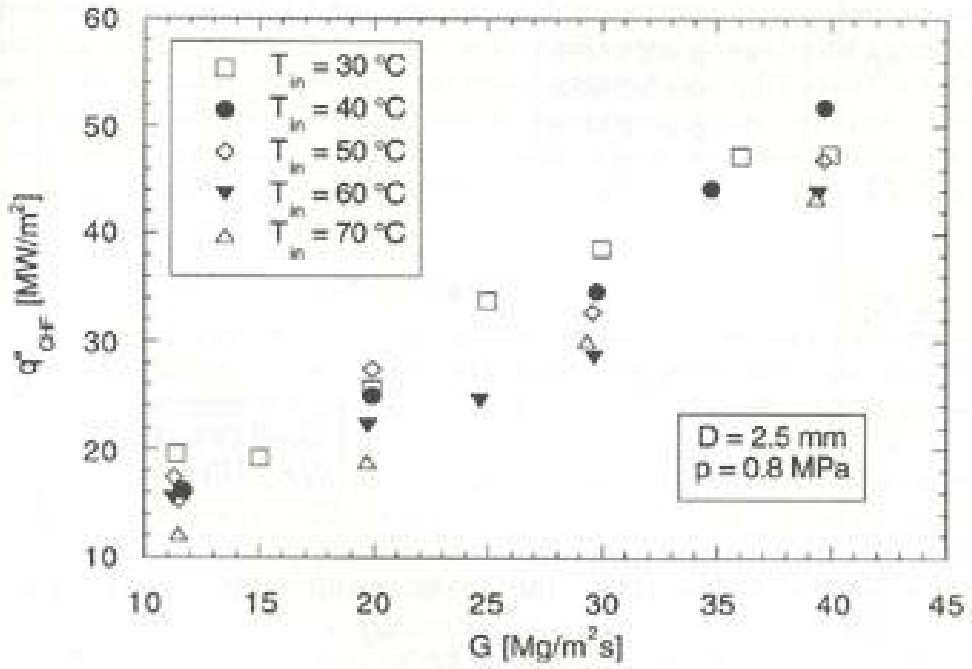

Fig. 2. Influence of mass flux on the CHF.

Mg/m²s) to 1.1 (at G = 40 Mg/m²s), while the absolute increase looks almost constant. This influence is quite relevant considering the reduced variation of the water inlet temperature, i.e. only 40 °C. The direct effect of subcooling on the CHF is shown in Fig. 3, where the CHF is plotted versus the inlet subcooling $\Delta T_{sub,in}$ for D = 8.0 mm. It is evident the almost linear dependence of the CHF on inlet subcooling. The slope of the curve on which data at a given pressure and liquid velocity would seem to lie does not depend on the two aforementioned parameters, i.e. p and u. This is in the sense that CHF versus $\Delta T_{sub,in}$ curves plotted at different liquid velocities result parallel among each other, and no inter-relation between u and $\Delta T_{sub,in}$ would seem to exist. Practical limits in the increase of the inlet subcooling are the system pressure (limited by the mechanical design of the fusion reactor at about 5.0 MPa) and the temperature of the heat sink (at present around 30-60 °C in the NET design).

4.3. *Effect of pressure*

From Fig. 3, it is possible to argue that, as CHF data versus $\Delta T_{sub,in}$ for different pressures lie on the same curve, the functional dependence of CHF from inlet subcooling is very slightly affected by the pressure. Direct influence of the pressure on CHF is observable in Fig. 4, where the CHF is plotted versus exit

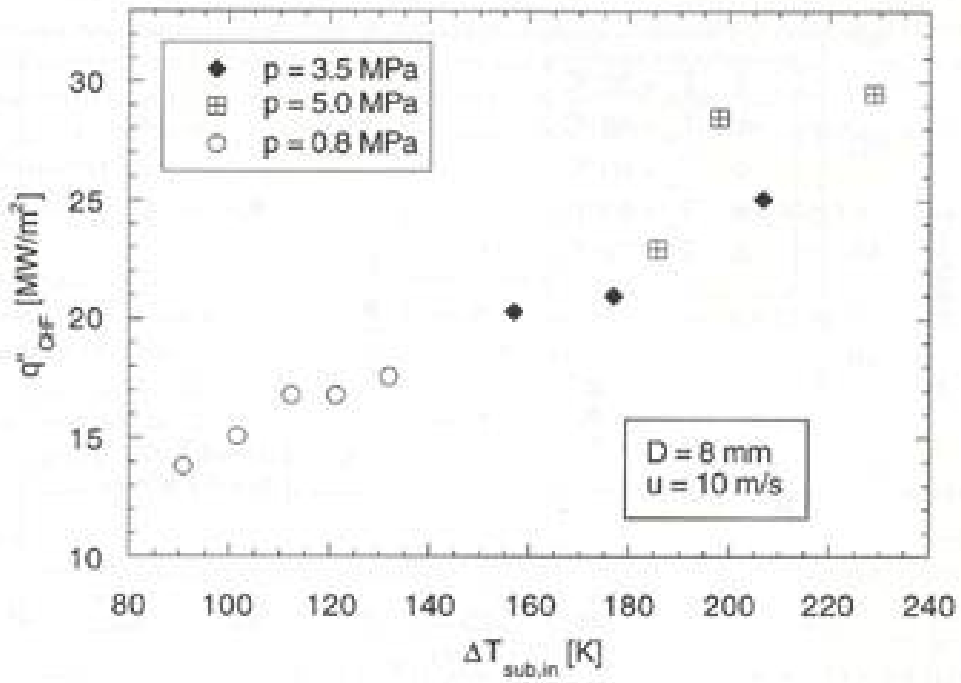

Fig. 3. Influence of inlet subcooling on the CHF

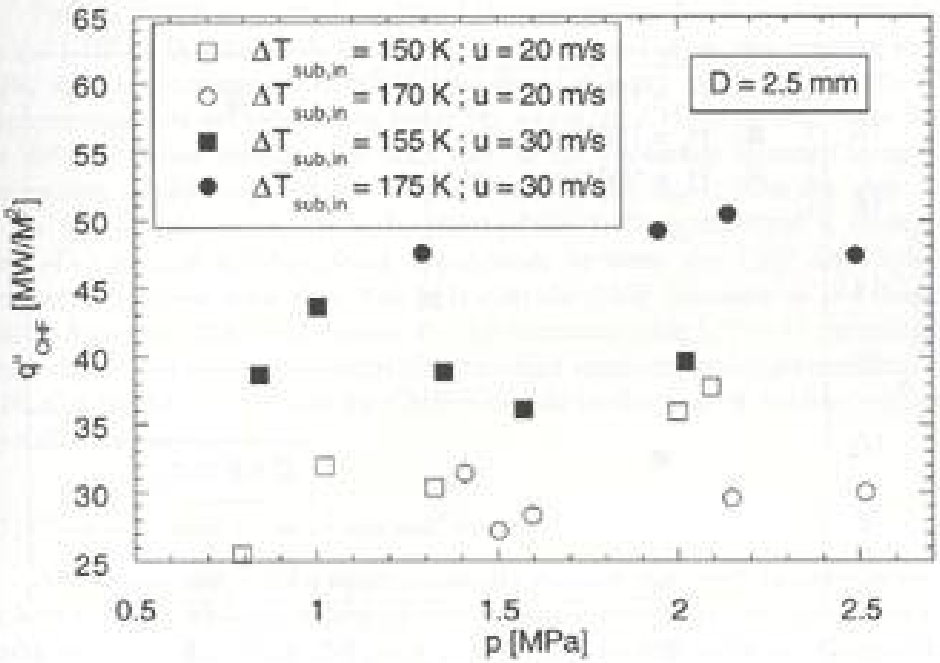

Fig. 4. Influence of pressure on the CHF.

pressure p, for the D = 2.5 mm data and for different values of liquid velocity and subcooling. The effect of the pressure on the CHF is negligible at least if compared with that of liquid velocity and subcooling, although the CHF shows a slight increasing dependence on the pressure. Nonetheless higher pressures, other conditions being equal, enable us to obtain higher liquid subcoolings and, indirectly, contribute to the enhancement of the CHF.

4.4. *Effect of channel length and orientation*

A point of relevant interest is the possible influence of the channel orientation and of the channel length on the CHF. Some tests were carried out with the purpose to ascertain this influence using D = 8.0 mm channels, and results are presented in Fig. 5a, where CHF is plotted versus mass flux. In the range of the tested liquid velocity (2 to 8 m/s) horizontal against vertical data do not show any appreciable difference, while an increase of 50% of the heated length in the vertical position does not affect the CHF. The first observation, i.e. the independence of the CHF from the orientation of the channel, is of interest for practical purposes of NET as the divertor is supposed to be inclined of about 30° from the horizontal and most of research is conducted with either vertical or horizontal test sections.

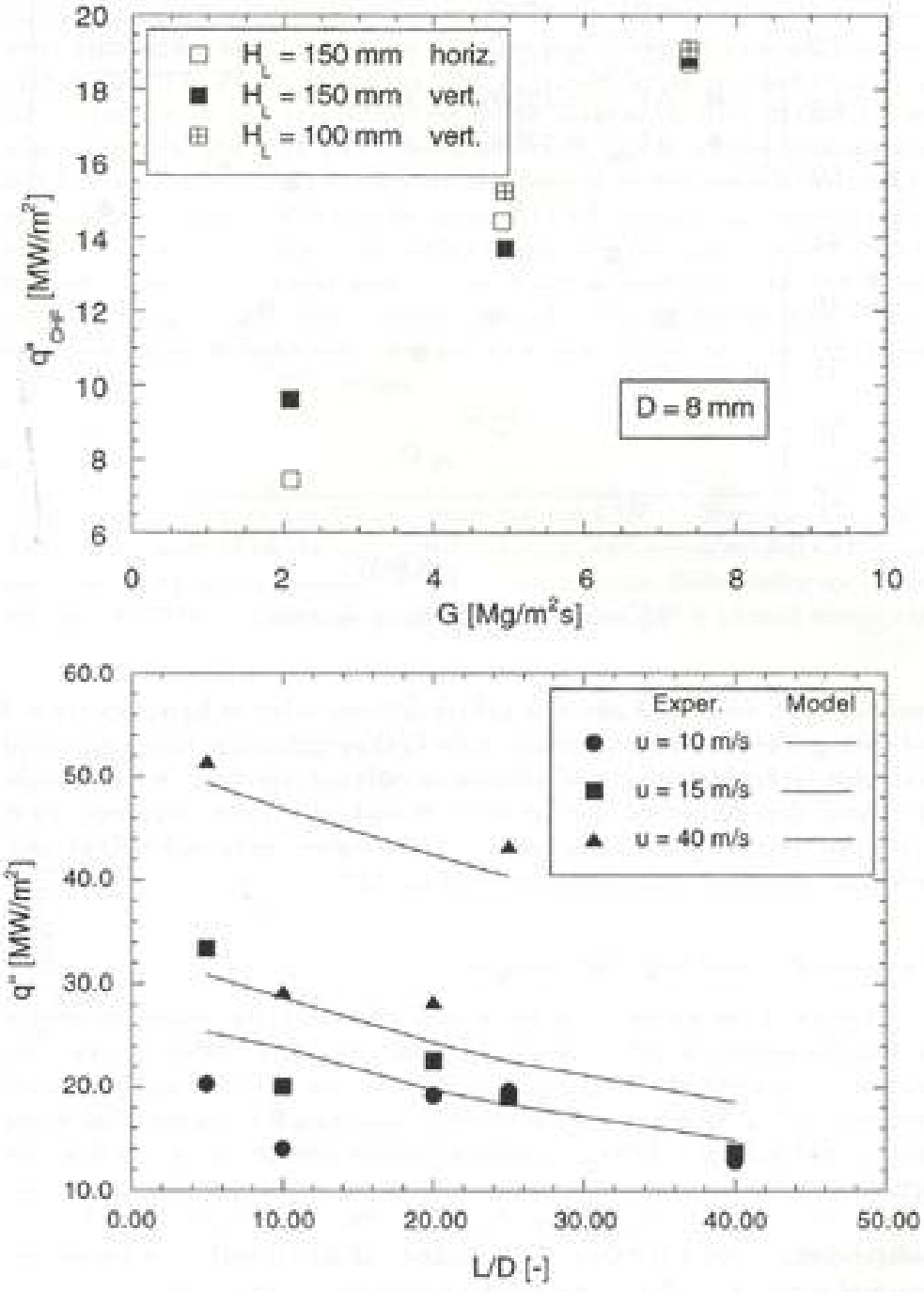

Fig. 5. Influence of channel orientation and lenght on the CHF.

Further tests were carried out later [21] to ascertain the channel length effect on the CHF. L/D ratios of 5, 10, 25 and 40 were tested at an exit pressure of 0.8 MPa, an inlet temperature of 60 °C and liquid velocity of 10, 15 and 40 m/s. Experimental data are reported in figure 5b, where the CHF is plotted versus L/D for different liquid velocity. The lines refer to the evaluation obtained using the mechanistic model proposed later in the present paper. Apart from the scattering of the liquid high velocity data, the effect of the L/D on the CHF is negligible for L/D > 30 and the functional dependence between the CHF and L/D is independent of the mass flux. For L/D < 30 the CHF increases as the channel length decreases. This result makes the achievements with L/D > 30 immediately applicable to full scale components. As the effect seems to be the greatest for L/D < 20, this would indicate that the CHF is related to the state of bubbly-boundary layer development [21].

4.3. *Effect of channel diameter and wall thickness*

A thorough analysis of a single parameter requires that other parameters are to be kept constant while increasing or decreasing the parameter that is the object of the analysis. In other words the exit pressure, the mass flux, the heated length and, above all in the case of subcooled flow boiling CHF, the exit quality (or the exit thermal hydraulic conditions) must be kept constant during the tests with different test channel diameters. Unfortunately, most of the data points available in the literature were carried out for purposes different from the evaluation of the test channel diameter influence per se, and therefore only few of them are "homogeneous" in the sense above described. Figure 6 reports CHF versus x_{ex} for different channel diameters and for fixed values of liquid velocity, exit pressure and heated length of the test section. In Fig. 6 experimental data with D = 3.0 mm are from Inasaka and Nariai [11] while all the other data are from Celata *et al.* [7]. For given values of outlet thermal hydraulic conditions, heated length, liquid velocity, CHF increases with the decrease of the tube inside diameter. From data reported in Fig. 6 we derived the direct dependence on D of the CHF, other conditions being equal. Such a derivation was obtained considering a continuous, ideal curve of the data plotted in Fig. 6, and reading on these curves the values of CHF corresponding at a fixed value of x_{ex}. Figure 7 represents the aforementioned dependence for Inasaka and Nariai data [11] (D = 3 mm) and Celata *et al.* [7] data (D = 2.5, 4.0, 5.0 and 8.0 mm). The threshold beyond which the effect of the tube inside diameter may be considered negligible is a function of the channel geometry and the thermal hydraulic conditions. At this stage of the research, available experimental data do not allow to draw any systematic and quantitative conclusion, but only to have a generic qualitative information on the feature of the dependence. To explain the observed dependence of the CHF from the tube inside diameter it is worth reporting here three different reasons proposed by Bergles

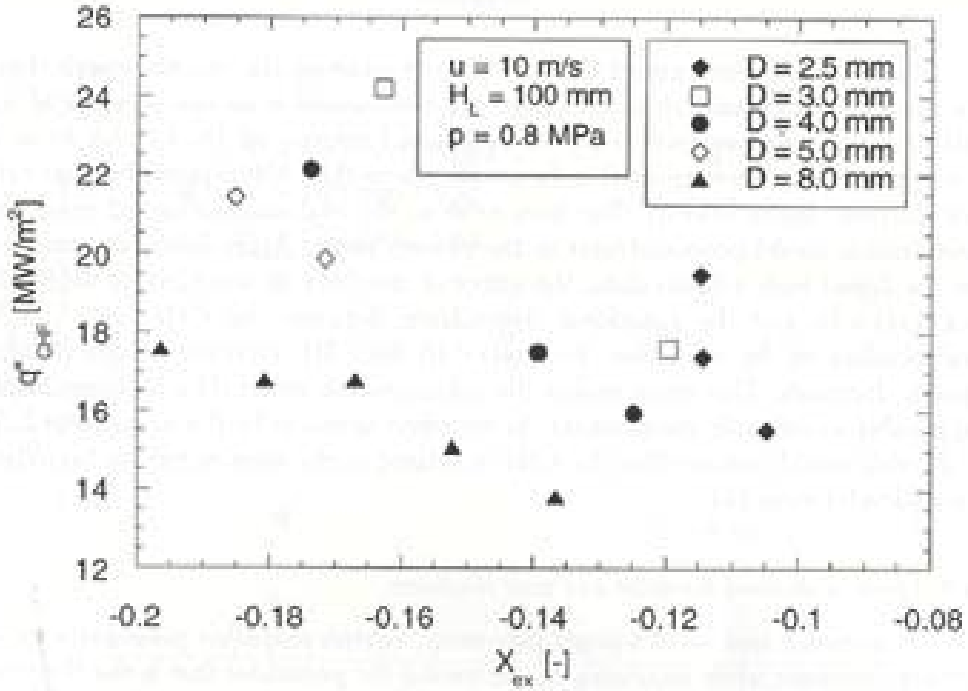

Fig. 6. Influence of channel diameter on the CHF (experimental data).

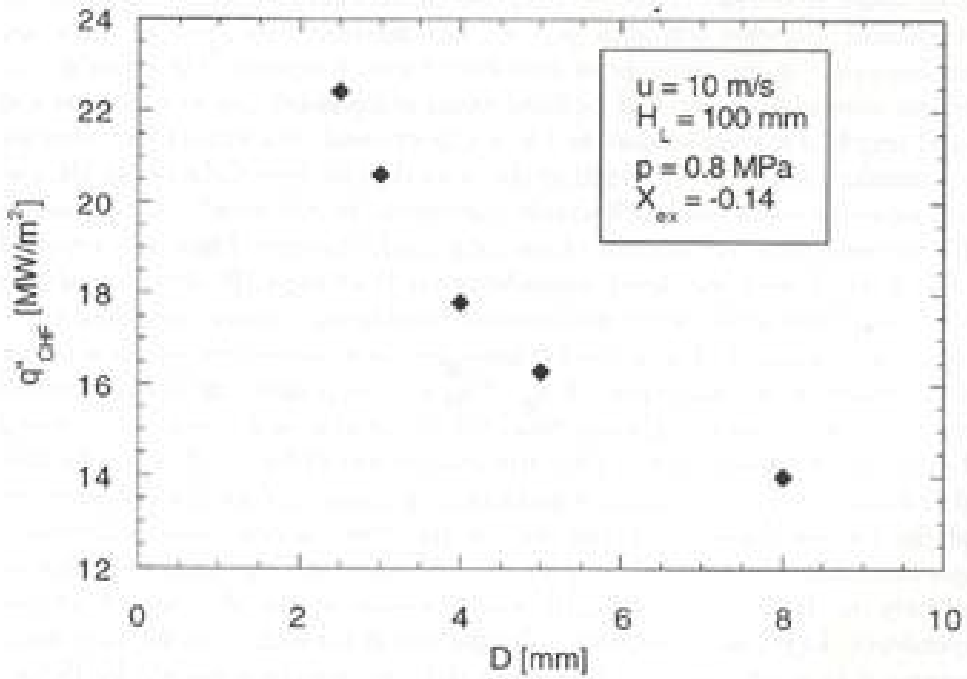

Fig. 7. Influence of channel diameter on the CHF (interpolated functional dependence).

[22]. For a tube with a smaller inside diameter we have: (i) a small bubbles diameter, (ii) an increased velocity of the bubbles with respect to the liquid, and (iii) the fluid subcooled bulk is closer to the growing bubbles (collapsing in the bulk).

Nariai and Inasaka [23] from the analysis of experimental data of void fraction in narrow tubes, concluded that, as tube inside diameter decreases and mass velocity increases, the diameter of generated bubble or, better, the thickness of the two-phase boundary layer becomes smaller due to the intense condensation effect by subcooled water at core region, and the void fraction becomes smaller, so to make the CHF higher. The decrease of the diameter gives rise to an increase of the slope of the velocity profile in the two-phase boundary layer, making the detachment of growing bubbles and the consequent condensation in the core region easier. The higher the mass flux the more consistent the above mentioned effect.

Additional tests were recently carried out ad hoc with the aim of ascertaining the functional dependence of the CHF on the channel diameter with special regard to very small diameter [21].

Tests, for a total of 42, were carried out under the following conditions:

— channel diameter, D	0.25, 0.5, 0.7, 1.2 and 1.5 mm
— liquid velocity, u	from 5 to 50 m/s
— exit pressure, p	from 0.1 to 0.8 MPa
— channel length, L	from 10 to 60 mm
— L/D	40
— inlet temperature, T_{in}	20 and 30 °C

Experimental data are reported in Fig. 8, together with predictions obtained using the already mentioned mechanistic model which will be reported later in this paper, based on the liquid sublayer dryout theory. Although an inverse dependence of the CHF from the channel diameter may be observed (for a given value of the exit quality), it is not easy to distinguish between 0.25, 0.5 and 0.7 mm data at atmospheric pressure. This means that the increasing trend of the CHF as the channel diameter decreases is not observed in present experiments for diameters below 0.7 mm. The comparison between the data and the model predictions is good for experimental data having $D \geq 0.7$ mm. On the contrary, a less accurate prediction is given for the smallest tubes, i.e., 0.25 and 0.5 mm. We may argue that below a given channel diameter, it is likely that the boiling crisis mechanism may be different from the liquid sublayer dryout theory. Indeed, we may think that as the channel diameter decreases we may face with bubbles whose size is of the same order of magnitude of the channel diameter itself.

As for channel diameter below 0.7 mm the bubble size may be thought to be of the same order of magnitude as the tube diameter, if we decrease the channel diameter it is reasonable to have a constant critical heat flux. Nonetheless, the possible 'flooding' of the channel by the vapour phase would justify the premature burnout with respect to the value obtained using the liquid sublayer dryout theory.

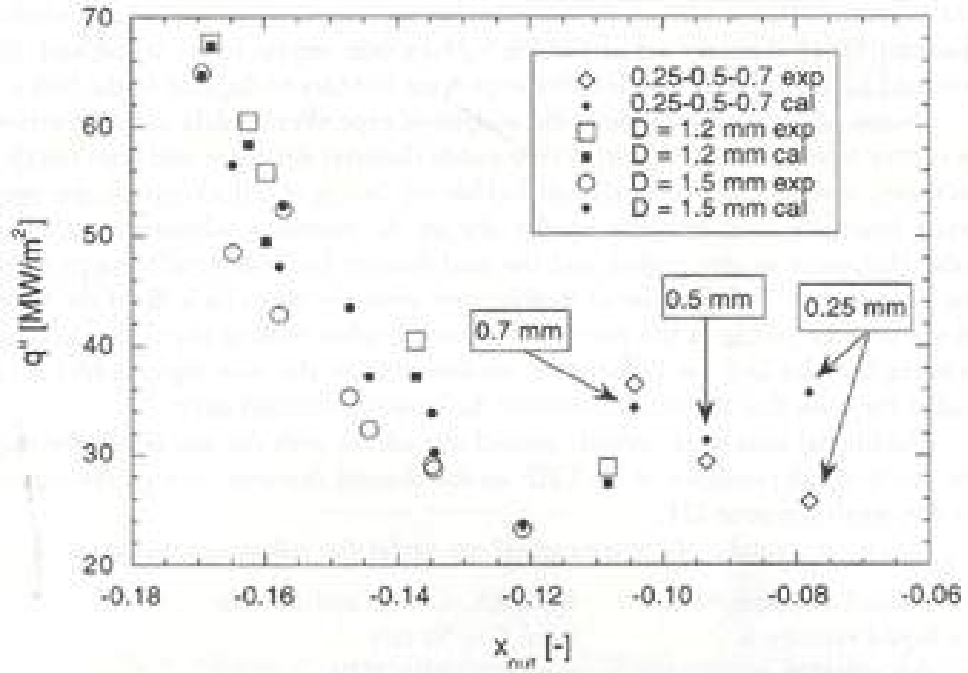

Fig. 8. CHF versus exit quality for small channel diameter tests; present data and comparison with the Celata *et al.* model.

Another important geometric parameter is the tube wall thickness. A specific experiment has been conducted using test sections having similar inner diameter and different tube wall thickness. Of course, tube material and exit thermal hydraulic conditions have been kept constant. The test matrix, for a total of 15 tests, has been the following:

— liquid velocity, u	30 m/s
— inlet temperature, T_{in}	30 °C
— exit pressure, p	0.8 MPa
— L/D	40
— inner diameter, D	from 1.61 to 1.74
— wall thickness, t	0.265, 0.38, 0.63, 0.945, and 1.195 mm

Experimental results are reported in Fig. 9 where the ratio between the calculated CHF (using the already mentioned mechanistic model which will be described later) and the experimental value is plotted versus the wall thickness. Considering the extended range of the wall thickness, up to a factor of six, its effect on the CHF may be regarded as very slight, even though a tendency to a an effect of the wall thickness may be evidenced for the thicker wall thicknesses.

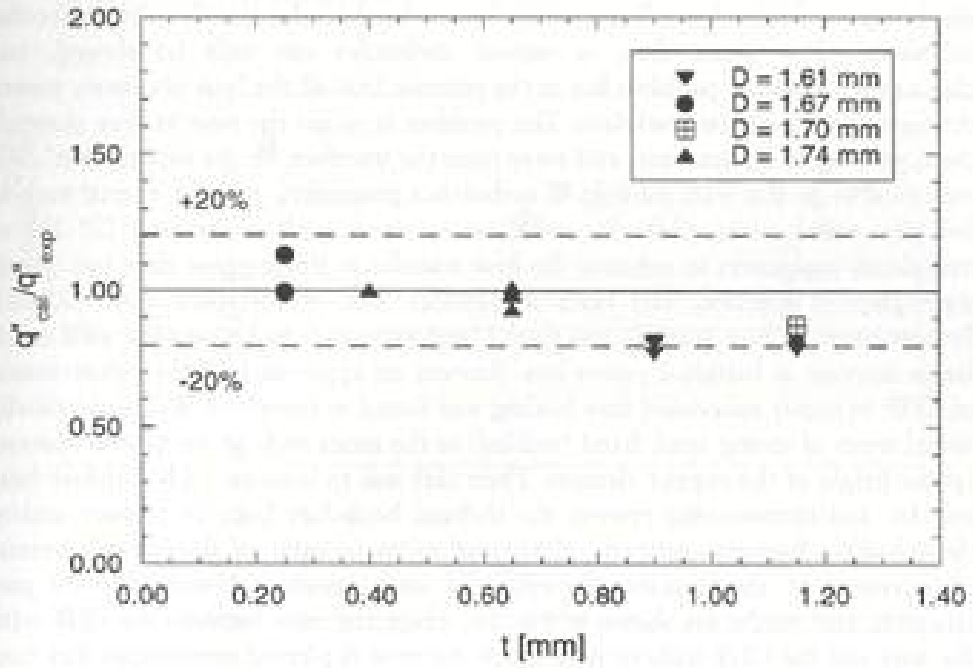

Fig. 9. Calculated-to-experimental CHF versus tube wall thickness.

4.6. Use of turbulence promoters for the enhancement of the CHF

The limit of 70 MW/m², maximum value of CHF reached in the above described experiments, is still a too low value if compared with what requested by fusion reactors thermal hydraulics designers, especially if we consider safety factors. On the other hand it is interesting to observe that according to Gambill and Lienhard [24] the CHF obtained is only around 1.5% of the maximum heat flux that can conceivably be achieved in a phase transition process. In fact, according to Gambill and Lienhard, "if one could contrive to collect every vapour molecule that leaves a liquid-vapour interface without permitting any vapour molecules to return to the liquid", the highest heat flux attainable can be estimated as:

$$\overset{''}{q}_{max} = \varrho_L \lambda \sqrt{\frac{RT}{2\pi}} \tag{3}$$

where R is the ideal gas constant on a unit mass basis. Under the conditions that allowed to reach a CHF of 60 MW/m², equation (3) provides a maximum theoretical heat flux of about 4000 MW/m². According to Gambill and Lienhard the most serious restriction that prevents reaching this limit in practice "is that

many vapour molecules will inevitably be returned to the interface by molecular collisions". The return flow of vapour molecules can only be slowed, not eliminated. "Another problem lies in the premise that all the heat ultimately passes through a liquid-vapour interface. The problem is to get the heat to flow through the liquid, up to an interface, and away from the interface on the vapour side". We contrived to do this with the help of turbulence promoters, or swirl inserts, such as helically coiled wires. Helically coiled wires were used in the past [25-28] as turbulence promoters to enhance the heat transfer in single-phase flow (air, water, water-glycerol solution, oil) both in laminar and in turbulent flow [25-28]. Enhancement of heat transfer was found (and expected) to be coupled with much larger increase in frictional power loss. Anyway no application to the enhancement of CHF in highly subcooled flow boiling was found in literature. We used helically coiled wires of spring steel, fixed (welded) at the inner ends of the heated channel (at the height of the copper clamps). Their task was to increase eddy diffusive heat transfer and continuously remove the thermal boundary layer to prevent and/or delay bubble formation/growth, giving rise to an increase of the overall thermal effectiveness of the coolant. Experiments were conducted with D = 8.0 mm channels, and results are shown in Fig. 10, where the ratio between the CHF with the wire and the CHF without wire inside the tube is plotted versus mass flux (top figure), and the ratio of the relative pressure drops is plotted always versus mass flux (bottom figure). Data are grouped according to the geometric characteristics of the wires. Unless differently specified data refer to 3.5 MPa, while data at 5.0 MPa refer to a wire diameter of 1.0 mm. The maximum increase of the CHF is up to a factor of about 1.5 for liquid velocities higher than 7.0 m/s, obtained with 1.0 mm diameter wire. Wires with smaller diameters would seem to be less effective on the CHF enhancement, perhaps because of a less mechanical stiffness to the force exerted by the fluid flow at these high velocities. Low velocity tests reveal very scattered and, as an average, a low efficiency in CHF enhancement. This is probably due to the fact that the relative roughness (wire diameter/hydraulic diameter of the channel) of the turbulence promoters determines the Reynolds number, and then the velocity, at which the promoters become effective, as stated by Sutherland [25] who established the heat transfer performance of boundary-layer turbulence promoters. The most efficient wire diameter for CHF enhancement is observed to be 1.0 mm, while the effect of relative spacing of promoters (pitch) can be considered negligible in the range 5-20 mm for the same wire. Sutherland observed a similar behaviour in the heat transfer performance. Nonetheless, pressure drop is inversely related to the wire pitch, as a pitch of 20.0 mm gives rise to an increase of the pressure drop (with respect to the smooth channel) of about 25% (1.0 mm wire diameter), while a pitch of 5.0 mm causes an increase of about 100%.

The effect of the pressure on the heat transfer performance (CHF enhancement) is observed to be negative, in the sense that tests carried out at 5.0

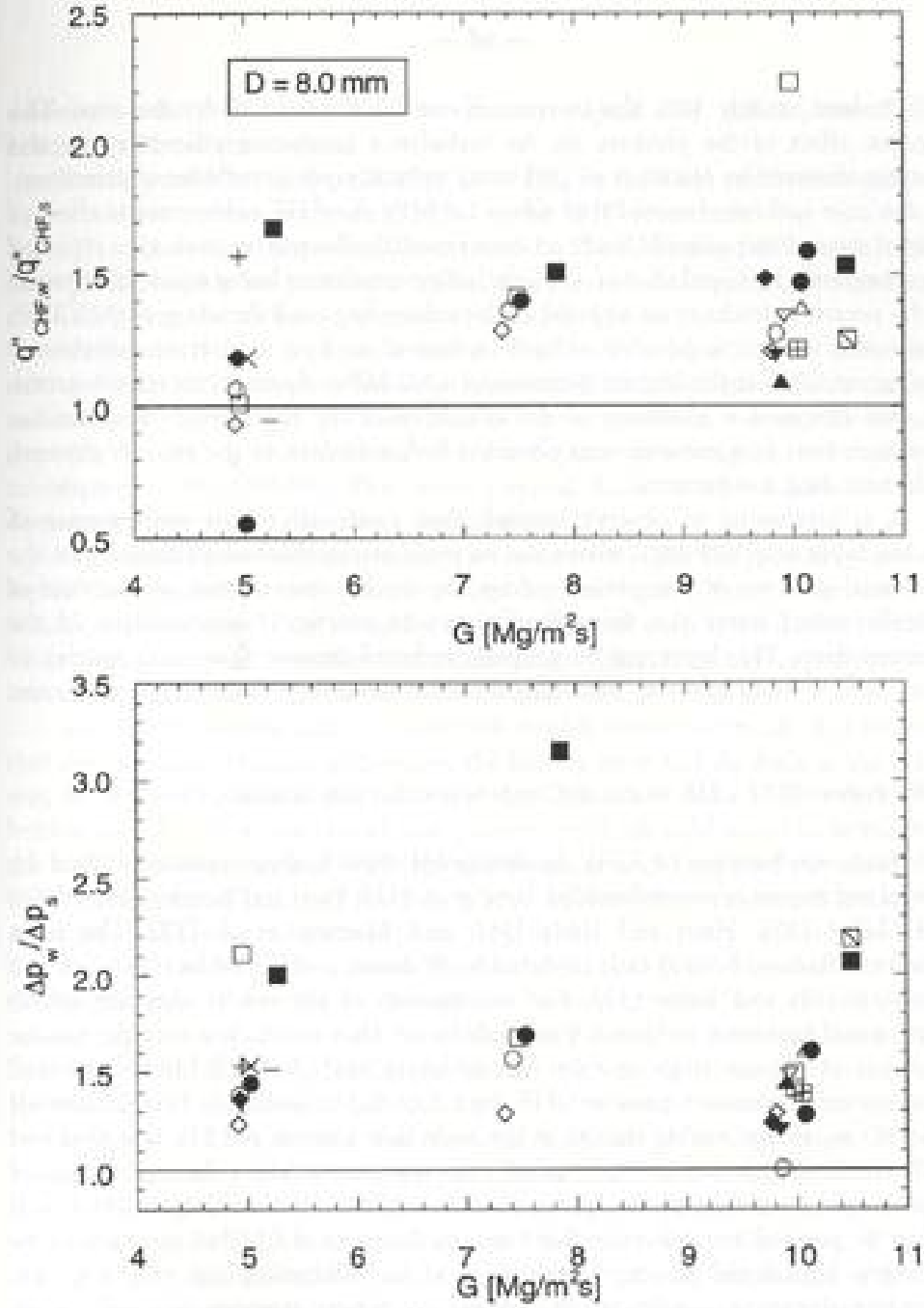

wire diameter [mm]	0.5	0.7	1.0	1.0
pitch [mm]	p [MPa] 3.5	3.5	3.5	5.0
1.5	–			
3.0	×			
5.0	□	⊞	■	⧅
7.5	–			
10.0	○	▲	●	△
15.0	+			
20.0	◇	▼	◆	▽

Fig. 10. Influence of helically coiled wires on the CHF (top figure) and on the pressure drop (bottom figure); if not specified data points refer to 3.5 MPa.

MPa reduce to only 30% the increase of the CHF produced by the wire. This negative effect of the pressure on the turbulence promoters efficiency was also recently observed by Nariai *et al.* [29] using twisted tapes as turbulence promoters. In that case authors observed that above 1.0 MPa the CHF enhancement effect of twisted tapes disappeared. Such an experimental observation was also reported experimentally by Gambill *et al.* [30]. As, other conditions being equal, an increase of the pressure produces an increase of the subcooling (and therefore of the CHF), in absolute terms it is possible to have (as indeed we have in present experiment) the highest CHF at the highest pressure (p = 5.0 MPa). Speaking in relative terms, we only observed a reduction in the efficiency of the turbulence promoter, i.e. maximum heat flux enhancement obtained with reference to the smooth channel, with increasing the pressure.

It is interesting to observe instead, that, contrarily to the performance of twisted tapes (e.g. [29-30]), where the increase of the thermal efficiency and the associated increase of the pressure drop are strictly inter-related, in the case of helically coiled wires the thermal efficiency is practically independent of the pressure drop. This latter can be properly reduced decreasing relative spacing of promoters, without affecting the thermal performance of the turbulence promoter.

5. Background of CHF modelling in subcooled flow boiling

Basic mechanisms of CHF in subcooled flow boiling, usually studied by optical techniques, were outlined by Tong *et al.* [33], Fiori and Bergles [34], Molen and Galjee [35], Hino and Ueda [36], and Mattson *et al.* [37]. The main achievements have been already reported by Weisman and Ileslamlou [18], Lee and Mudawar [19] and Katto [32]. For convenience of the reader they are briefly summarized hereafter: i) through photography or other means, it was evidenced the existence of vapour slugs or thin vapour layers near the wall [33-36]; ii) wall temperature fluctuations prior to CHF were detected in uniformly heated channels [38]; iii) no abrupt visible change in the bulk flow pattern at CHF was observed [37]; iv) the largest bubbles or vapour slugs are generated by the coalescence of smaller bubbles within the two-phase boundary layer in the wall region [35-37]. It has to be pointed out, however, that basic mechanisms of CHF in subcooled flow boiling at high liquid velocity (up to 40 m/s) and subcooling (up to 250 K), i.e. including operating conditions of interest to fusion reactors, are still to be understood, in spite of the many experimental data carried out in the recent past [4]. The great difficulty in applying optical techniques under the above thermal hydraulic conditions, that means fast and very small bubbles (whose diameter is around some microns or tens of microns), still prevents us to obtain the necessary information. What remains to be excluded is the hidden existence of an alternative crisis mechanism due to the sudden coalescence of wall tiny bubbles which, still

adhering to the wall and beneath the transient vapour slug, isolate thermally the heating wall from the coolant.

Existing models may be classified according to the basic mechanism assumed by the relative authors as the main cause of the CHF occurrence.

(1) Liquid layer superheat limit model. The difficulty of heat transport through the bubbly layer causes a critical superheat in the liquid layer adjacent to the wall, giving rise to the occurrence of the CHF [38].

(2) Boundary layer separation model. This model is based on the assumption that an "injection" of vapour from the heated wall into the liquid stream causes a reduction of the velocity gradient close to the wall. Once the vapour effusion increases beyond a critical value, the consequent flow stagnation is assumed to originate CHF [39-44]. The weak physical basis of the model has been demonstrated by the studies above reported [34-37].

(3) Liquid flow blockage model. It is assumed that the CHF occurs when the liquid flow normal to the wall is blocked by the vapour flow. Bergel'son [45] considers a critical velocity raised by the instability of the vapour-liquid interface, while Smogalev [46] considers the effect of the kinetic energy of vapour flow overcoming that of the counter motion of liquid.

(4) Vapour removal limit and near-wall bubble crowding model. It is assumed that the turbulent interchange between the bubbly layer and the bulk of the liquid may be the limiting mechanism leading to the CHF occurrence. CHF occurs when bubble crowding near the heated wall prevents the bulk cold liquid from reaching the wall [47]. Weisman and Pei [48], and Weisman and Ying [49] postulates that CHF occurs when the void fraction in the bubbly layer, calculated under the assumption of homogeneous two-phase flow in the bubbly layer in [48] and using the slip model in [49], just exceeds the critical value of 0.82. The void fraction in the bubbly layer is determined through the balance between the outward flow of vapour bubbles and the inward liquid flow at the bubbly layer-bulk liquid flow interface. Weisman and Ileslamlou model [18] is an improvement of Weisman and Pei model, for subcooled exit conditions. A research work carried out by Styrikovich *et al.* [30], showed that measured void fraction at CHF ranges from as low as 0.3 to as high as 0.95, making the validity of the near-wall bubble crowding models questionable. In addition, the models are quite empirical in the determination of the turbulent exchange in the bubbly layer. Obviously, it is not excluded that, due to differences in the thermal hydraulic conditions, different crisis mechanisms may verify and so to be valid in some ranges of the above conditions.

(5) Liquid sublayer dryout model. The model is based on the dryout of a thin liquid sublayer underneath a vapour blanket or elongated bubble, due to coalescent bubbles, flowing over the wall. This model is supported by more recent experimental studies [35-37], [51-54] in the conditions of our interest.

Lee and Mudawar [19] proposed a mechanistic sublayer dryout model which

eliminates the need for much of the empiricism found in above described subcooled flow boiling CHF models. Unlike most of them, the CHF analysis proposed by Lee and Mudawar is theoretically based, requiring only three empirical constants. The model closely predicts several well known CHF data bases at high pressure (above 5.0 MPa). Nonetheless, as some assumptions are not valid for low pressure systems (such as the NET divertor), it is not expected to yield accurate CHF predictions at low pressure [31].

Recently, Katto [32] proposed a model for the prediction of subcooled flow boiling CHF in a very extended range of pressure (0.1-20.0 MPa), employing essentially the same theoretical model constructed by Lee and Mudawar. Main differences are in the calculation of the vapour blanket velocity, obtained by an empirically-based relation (as a function of Reynolds number, liquid and vapour density, and void fraction), and in the evaluation of the liquid sublayer thickness, that was indirectly modelled using a correlation for pool boiling [55]. The Katto model, although yielding acceptable predictions of very high heat fluxes CHF data points in a wide range of pressure, is not able to calculate the CHF in those cases where the local void fraction in the near-wall bubbly layer is higher than 70%. This is the limit considered by the author for the validity of the assumption of homogeneous flow in the bubbly layer. It happens in all cases where inlet thermal hydraulic conditions are such that the bulk liquid at the exit is slightly subcooled, and was verified for about 51% of high heat flux CHF data collected so far in the literature [31].

Considering that the Lee and Mudawar model cannot be properly used at low pressure, and in view of the above described limitations of the Katto model, a new model has been developed with the aim of overcoming above inconvenients.

6. The proposed CHF model

The basic assumptions which the proposed model is based on, are exactly the same used by Lee and Mudawar [19] and by Katto [32] (liquid sublayer dryout model), and also some of the definitions reported below are borrowed from them. The reference flow configuration is schematically illustrated in Fig. 11. A thin elongated bubble, called "vapour blanket", is formed as a consequence of coalescence of small bubbles rising along the near-wall region as vertical distorted vapour cylinders. The vapour blanket is overlying a very thin liquid sublayer adjacent to the wall, and CHF is assumed to occur when the liquid sublayer initial thickness, δ is extinguished by evaporation during the passage time of the vapour blanket, $\tau = L_b/U_b$, where L_b and U_b are the length and velocity of the vapour blanket, respectively.

As assumed by Lee and Mudawar [19], the circumferential growth of a vapour blanket is strongly limited by adjacent blankets. It is therefore reasonable to assume

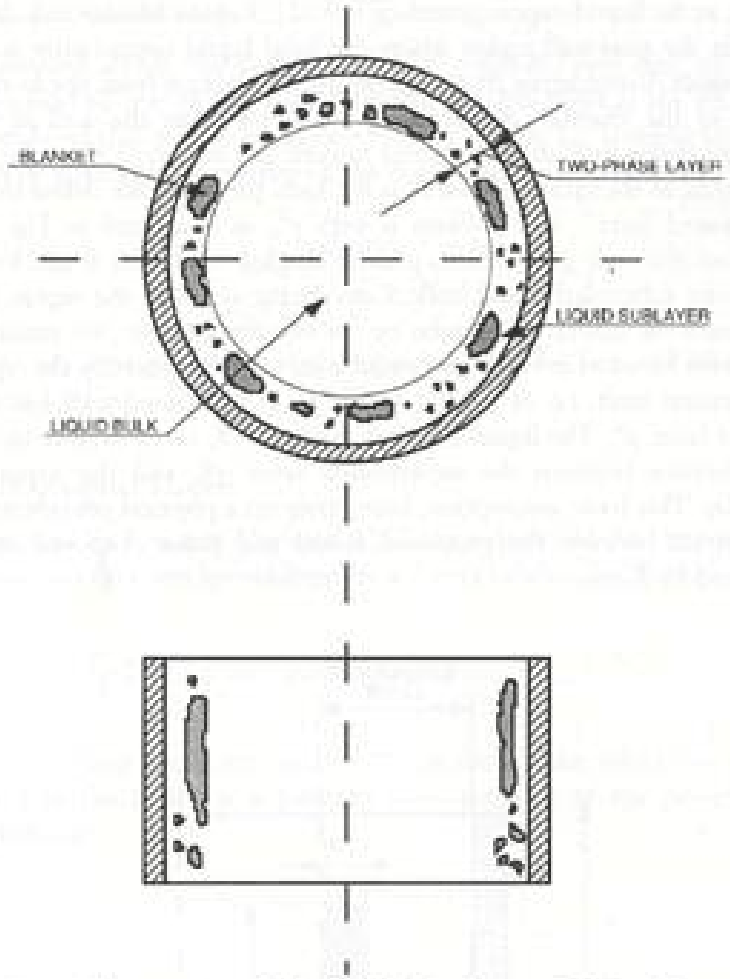

Fig. 11. Schematization of subcooled flow boiling near CHF conditions.

the equivalent diameter of each blanket, D_g (i.e. its thickness) as approximately equal to the diameter of a bubble at the departure from the wall. It is assumed that departing bubbles may coalesce into a distorted blanket that stretches along the fluid flow direction (due to vapour generation by sublayer evaporation) and keeps almost a constant equivalent diameter (thickness). A continuous blanket may be formed along the inner wall of the tube, as a consequence of circumferential blankets merging. Vapour blanket velocity, U_g, is obtained by superimposing the liquid velocity, calculated using the velocity universal profile, and the relative blanket velocity, with respect to the liquid, deduced from a forces balance applied to the blanket (buoyancy and drag) [19].

Vapour blanket length, L_g, is postulated to be equal to the critical Helmholtz

wavelength at the liquid-vapour interface [19-32]. Vapour blanket can develop and exist only in the near-wall region where the local liquid temperature is above the saturation value. Considering the temperature distribution from the heated wall to the center of the channel, it will exist a distance from the wall at which the temperature, decreasing as we proceed toward the center of the tube along the radius, is equal to the saturation value at the local pressure. We define this distance as "superheated layer", and indicate it with y^*, as illustrated in Fig. 12. For a distance from the wall greater than y^*, the blanket (and each single bubble) will collapse in the subcooled liquid bulk. Considering also that the vapour blanket is pushed toward the center of the tube by the velocity gradient, we assume that the vapour blanket location in the superheated layer is such to occupy the region closer to the saturation limit, i.e. as far as possible from the heated wall, but within the superheated layer, y^*. The liquid sublayer thickness, δ, can therefore be calculated as the difference between the superheated layer, y^*, and the vapour blanket thickness, D_b. This basic assumption, based only on a physical consideration, is the main difference between the proposed model and those proposed by Lee and Mudawar and by Katto.

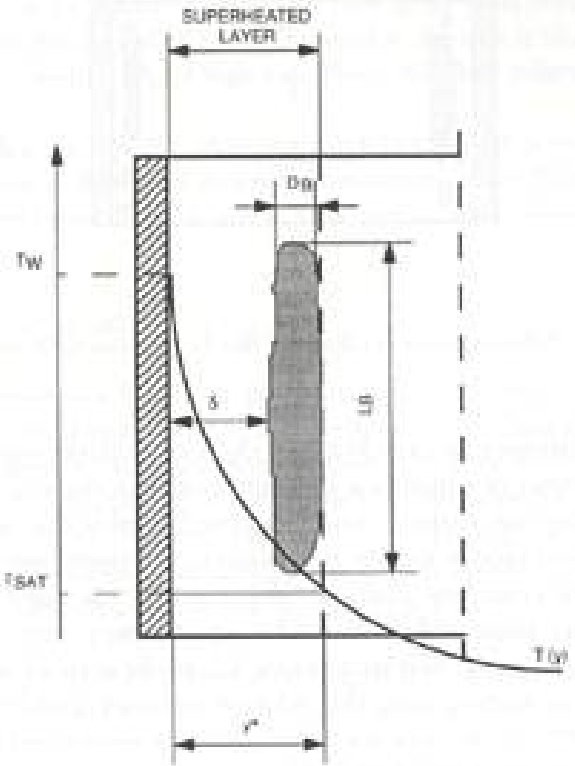

Fig. 12. Schematization of the superheated layer, i.e. the two-phase layer.

6.1. Length of vapour blanket

As discussed above, the liquid sublayer is generally very thin, and it can be roughly assumed to rest on the wall, while the blanket flows at the velocity U_B. It is then postulated that the mean vapour blanket length, L_B, is equal to the critical wavelength of Helmholtz instability of the liquid-vapour interface, and is given by:

$$L_B = \frac{2\pi\sigma(\varrho_V + \varrho_L)}{\varrho_V \varrho_L U_B^2} \tag{4}$$

This is the same procedure and expression used by Lee and Mudawar [19] and by Katto [32].

6.2. Velocity of vapour blanket

As reported by Lee and Mudawar [19], the velocity of the vapour blanket in vertical turbulent flow can be obtained by a forces balance, i.e. buoyancy and drag forces:

$$\frac{\pi}{4} D_B^2 L_B g (\varrho_L - \varrho_V) = \frac{1}{2} \varrho_L C_D (U_B - U_{BL})^2 \frac{\pi D_B^2}{4} \tag{5}$$

where C_D is the drag coefficient and U_B-U_{BL} is the relative velocity of the blanket with respect to the liquid at a position corresponding to the centerline of the blanket, given by:

$$U_B - U_{BL} = \left(\frac{2 L_B g (\varrho_L - \varrho_V)}{\rho_L C_D} \right)^{0.5} \tag{6}$$

The drag coefficient, C_D, is calculated using the equation recommended by Harmathy [56] and Ishii and Zuber [57] for a deformed bubble the motion of which is determined by buoyancy and surface tension forces, given by:

$$C_D = \frac{2}{3} \frac{D_B}{\left(\frac{\sigma}{g(\varrho_L - \varrho_V)} \right)^{0.5}} \tag{7}$$

For the evaluation of the vapour blanket equivalent diameter, or thickness, D_B, it was used the model proposed by Staub [58], based on a balance of forces to growing bubbles attached to the heated surface, to approximate diameter of bubbles at departure. In the model, the bubble is considered to detach from the surface when dislodging forces overcome adhesive forces. Among the several forces acting on the bubble (surface tension force, dynamic force due to the momentum

change of the liquid resulting from the growing bubble, drag force, buoyancy force, dynamic forces due to the liquid inertia and to the evaporating vapour thrust), Staub considered surface tension force (adhesive) and drag force (dislodging) to be the dominant, and the balance of such forces yields the following expression for D_b:

$$D_b = \frac{32}{f} \frac{\sigma f(\beta) \varrho_L}{G^2} \tag{8}$$

where β is the contact angle, and $f(\beta)$ is a function that depends only on contact angle. An approximate value for $f(\beta)$ of 0.02 to 0.03 for water was recommended, and $f(\beta) = 0.03$ is used in the present model.

The friction factor f, is calculated using the Colebrook-White equation combined with Levy's rough surface model [59], recommended for highly subcooled nucleate boiling. In fact, the pressure drop gradient will increase in the proximity of the CHF, as the bubbles cause an increased surface roughness, but the coolant will still behave as a single-phase fluid. The expression for the friction factor is given by:

$$\frac{1}{\sqrt{f}} = 1.14 - 2.0 \log\left(\frac{\varepsilon}{D} + \frac{9.35}{Re\sqrt{f}}\right) \tag{9}$$

where ε is the surface roughness, that has been shown to be close to 0.75 D_b, D is the inner tube diameter, and Re is the Reynolds number. Considering that $f(\beta) = 0.03$ and that $\varepsilon = 0.75\ D_b$, the above equation, making use of eq. (8), becomes:

$$\frac{1}{\sqrt{f}} = 1.14 - 2.0 \log\left(\frac{0.72\, \sigma \varrho_L}{fDG^2} + \frac{9.35}{Re\sqrt{f}}\right) \tag{10}$$

Note the dependence of the friction factor on the surface tension. Solution of this equation for the friction factor requires iteration.

Turning to the calculation of U_g, eq. (6), it is now necessary to calculate U_{gL}, i.e. the liquid velocity, U_L, at the center-line of the vapour blanket. The liquid velocity, U_L, for a turbulent flow in a tube as a function of the distance from the wall, y, can be represented by the Karman velocity distribution as

$$U_L^+ = y^+ \qquad 0 \le y^+ < 5 \tag{11}$$

$$U_L^+ = 5.0 \ln y^+ - 3.05 \qquad 5 \le y^+ < 30 \tag{12}$$

$$U_L^+ = 2.5 \ln y^+ + 5.5 \qquad y^+ \ge 30 \tag{13}$$

where:

$$U_L^+ = \frac{U_L}{U_\tau} \qquad U_\tau = \left(\frac{\tau_w}{\varrho_L}\right)^{0.5} \qquad y^+ = y\,\frac{U_\tau}{\mu_L}\varrho \qquad \tau_w = \frac{fG^2}{8\varrho_L}$$

Calculating U_{BL} as the mean liquid velocity, U_L, at distance $y = \delta + D_B/2$ from the wall using eqs. (11) - (13), and rearranging eq. (6) the vapour blanket velocity, U_B, is given by:

$$U_B = \left(\frac{2L_B\, g\,(\varrho_L - \varrho_V)}{\varrho_L C_D}\right)^{0.5} + 0.125\,(\delta + \frac{D_B}{2})\,\frac{fG^2}{\varrho_L \mu_L} \tag{14a}$$

$$U_B = \left(\frac{2L_B\, g\,(\varrho_L - \varrho_V)}{\varrho_L C_D}\right)^{0.5} + 1.768\sqrt{f}\,\frac{G}{\varrho_L}\left\{ln\left[0.354\,\frac{G}{\mu_L}\sqrt{f}\left(\delta + \frac{D_B}{2}\right)\right] - 0.61\right\} \tag{14b}$$

$$U_B = \left(\frac{2L_B\, g\,(\varrho_L - \varrho_V)}{\varrho_L C_D}\right)^{0.5} + 0.884\sqrt{f}\,\frac{G}{\varrho_L}\left\{ln\left[0.354\,\frac{G}{\mu_L}\sqrt{f}\left(\delta + \frac{D_B}{2}\right)\right] + 2.2\right\} \tag{14c}$$

The procedure adopted for the calculation of the vapour blanket velocity is the same as Lee and Mudawar [19], while the equations used for the evaluation of the blanket equivalent diameter, or thickness, and the friction factor are different. Those used in the Lee and Mudawar model are not suitable for the operating ranges which the present model is intended to.

6.3. *Initial thickness of liquid sublayer*

As already discussed, the thickness of the liquid sublayer is calculated as the difference between the superheated layer, y^+, and the vapour blanket thickness, or equivalent diameter, D_B:

$$\delta = y^+ - D_B \tag{15}$$

as D_B can be calculated by eq. (8), it is now necessary to calculate the distance from the wall at which the temperature is equal to the saturation value. The temperature T at a given distance from the wall y, can be obtained using the temperature distribution for turbulent flow in a tube, as proposed by Martinelli [60]:

$$T(y^+) = T_w - QPr\,y^+ \qquad 0 \le y^+ < 5 \tag{16}$$

$$T(y^+) = T_w - 5Q\left\{Pr + ln\left[1 + Pr\left(\frac{y^+}{5} - 1\right)\right]\right\} \qquad 5 \le y^+ < 30 \tag{17}$$

$$T(y^+) = T_w - 5Q\left[Pr + ln\,(1+5Pr) + 0.5\,ln\left(\frac{y^+}{30}\right)\right] \qquad y^+ \geq 30 \qquad (18)$$

where T_w is the wall temperature, Pr is the liquid Prandtl number, y^+ is defined above, and Q is a group defined as a function of the local heat flux, q'', the liquid specific heat, C_{pL}, and the friction velocity, U_τ:

$$Q = \frac{q''}{\rho_L C_{pL} U_\tau} \qquad (19)$$

As the wall temperature T_w is not known (it can only be calculated using empirical correlations), the calculation of the temperature distribution is based on the exit average temperature of the fluid, T_m. This latter is calculated, for a given heat flux q'', by the heat balance in the fluid:

$$T_m = T_{in} + \frac{q'' S}{\Gamma C_{pL}} \qquad (20)$$

where T_{in} is the liquid inlet temperature, S is the heat transfer surface ($S = \pi DL$), and Γ is the mass flow rate. The average temperature T_m, obtained from eq. (20), can be put equal to that calculated using eqs. (16) through (18):

$$T_m = \frac{5}{y^+(R)} T_{m1} + \frac{25}{y^+(R)} T_{m2} + \frac{y^+(R) - 30}{y^+(R)} T_{m3} \qquad (21)$$

being

$$T_{m1} = \frac{1}{5}\int_0^5 T(y^+)dy^+ \qquad 0 \leq y^+ < 5 \qquad (22)$$

$$T_{m2} = \frac{1}{25}\int_5^{30} T(y^+)dy^+ \qquad 5 \leq y^+ < 30 \qquad (23)$$

$$T_{m3} = \frac{1}{y^+(R) - 30}\int_{30}^{y^+(R)} T(y^+)dy^+ \qquad y^+ \geq 30 \qquad (24)$$

and R the radius of the channel. In eq. (21), T_w is the only unknown and, therefore, it can be determined. Once T_w is known, it will be possible to calculate the distance from the wall y, at which the liquid temperature is equal to the saturation value at the local pressure, i.e. the superheated layer y^*. Now calculating D_B from eq. (8), and from the knowledge of y^*, it is possible to calculate the liquid sublayer thickness δ, from eq. (15).

This procedure is different from Lee and Mudawar, and Katto models, and allows to obtain the wall temperature directly from the heat balance, without making use of empirical correlations for the evaluation of the heat transfer coefficient as well as of empirical constants.

6.4. *Critical heat flux*

The critical heat flux, CHF, is calculated according to the procedure proposed by Katto [32]. The minimum heat flux necessary to extinguish a liquid sublayer of initial thickness δ by evaporation during the passage time τ of a vapour blanket having a velocity U_B and a length L_B, is:

$$CHF = \frac{\varrho_L \delta \lambda}{\tau} = \frac{\varrho_L \delta \lambda}{L_B} U_B \tag{25}$$

where ϱ_L and λ are the liquid density and the latent heat of vaporization, respectively, both calculated at saturated conditions. Thus, for given geometric and inlet thermal hydraulic conditions, and local pressure p, the critical heat flux CHF can be predicted by an iterative procedure through the foregoing equations (4), (7), (8), (10) through (21), and (25).

7. Verification of the CHF model

To verify the accuracy of the proposed model, a CHF data base recently gathered by authors under operating ranges typical of fusion reactor thermal hydraulics was used. The data set [7-13, 61] was based on 1888 data points and was detailed in [31], where it was used by present authors to assess existing correlations and models for the prediction of water subcooled flow boiling CHF at high liquid velocity and subcooling. The data base covers the following operating ranges: $0.1 \leq p \leq 8.4$ MPa; $0.3 \leq D \leq 25.4$ mm; $0.0025 \leq L \leq 0.61$m; $1 \leq G \leq 90$ Mg/m²s; $25 \leq \Delta T_{sub,in} \leq 255$ K.

Figure 13 shows a comparison of calculated versus experimental CHF, using the above data set. About 91% of data points are predicted within ± 30%, with an r.m.s. of 17.2%. This is a good performance, also taking into account the wide operating ranges of the data set. With reference to the results reported in [31], a

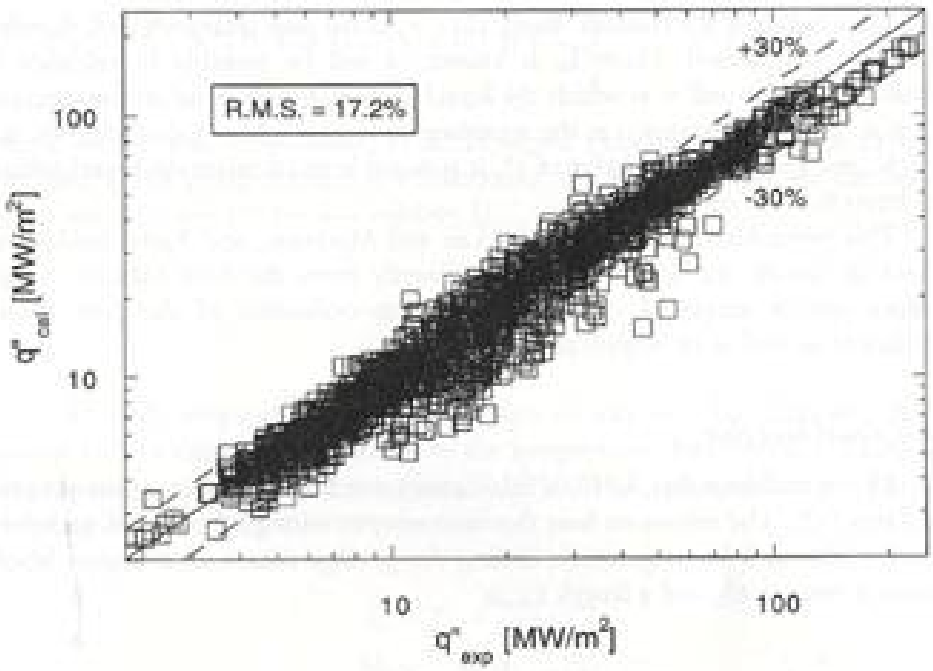

Fig. 13. Calculated versus experimental CHF using the whole data set [7-13][61].

comparison between the performances of the Katto model [32] and of the present model has been accomplished. The percentage of data points calculated with a given error band (%) is plotted in Fig. 14 against the error band, for the two models. The proposed model provides better predictions than the Katto model all over the error band range, with particular emphasis to the region ± 10% - ± 30%. The present model (24.5%).

There is also another significant difference between the two models regarding the number of data points that they are able to predict. While the proposed model is able to calculate all the 1888 data points, the Katto model fails for 961 data points (50.9%). They are discarded because the calculation procedure of the Katto model requires the void fraction in the boiling layer be less than 0.7. This condition is matched whenever the inlet subcooling is medium/low and is associated with low liquid velocity. This is the limit considered by the author for the validity of the assumption of homogeneous flow in the near-wall, two-phase boundary layer. For conditions where a void fraction higher than 0.7 is predicted in the calculation procedure, the model cannot calculate the CHF. Figures 15 through 17 show the ratio between calculated and experimental CHF versus thermal hydraulic conditions (G, p, x_{ex}), to ascertain possible systematic effects in the model behaviour.

A slight underprediction of the CHF can be observed for mass flux lower than 2 Mg/m^{2}s, however in a region where the CHF is not high (Fig. 15), that is beyond

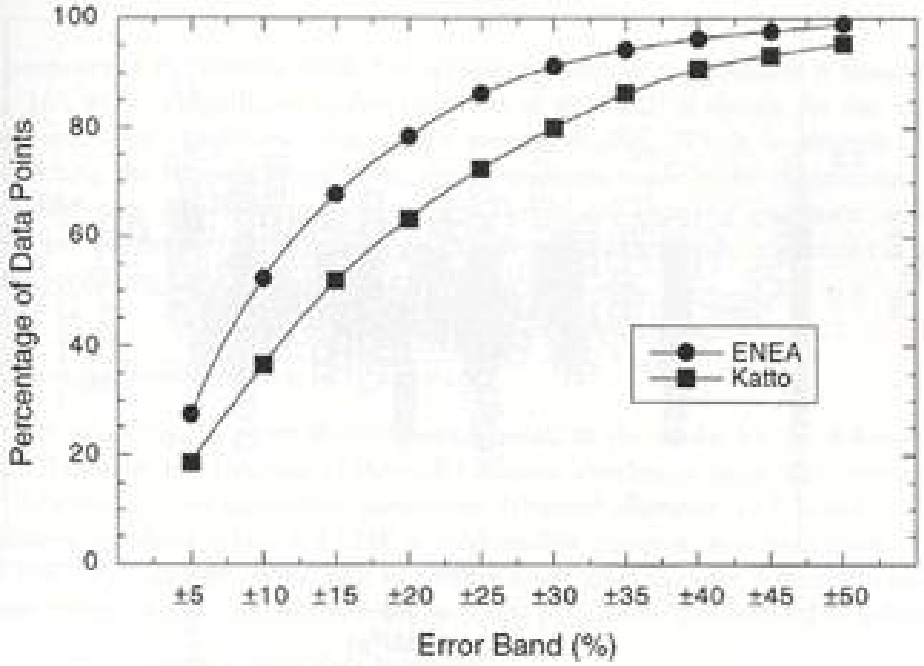

Fig. 14. Percentage of data points predicted within a given error band versus the error band, for the present model and the Katto model [32].

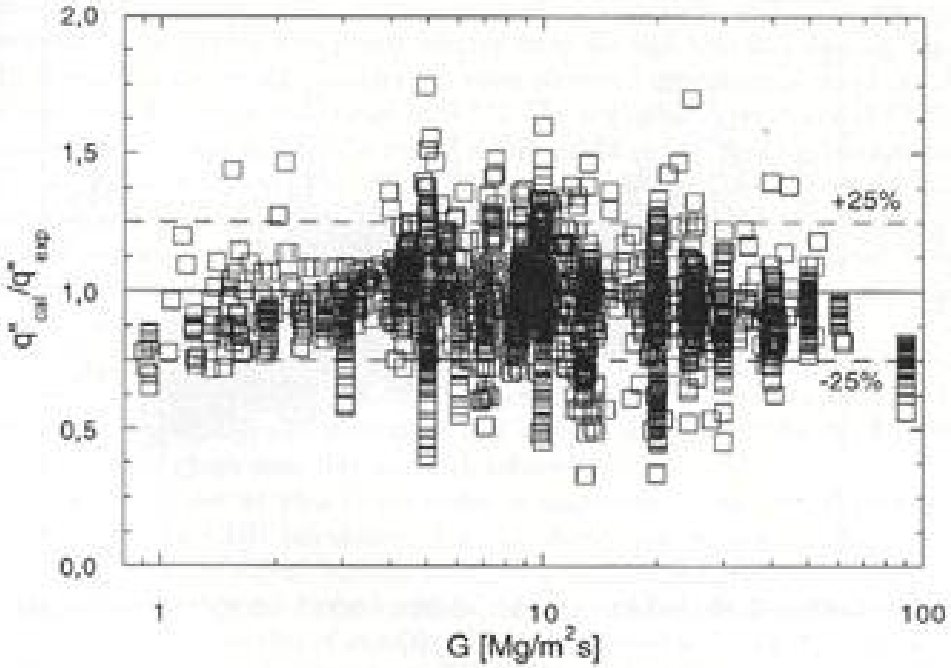

Fig. 15. Ratio of the calculated to the experimental CHF versus mass flux.

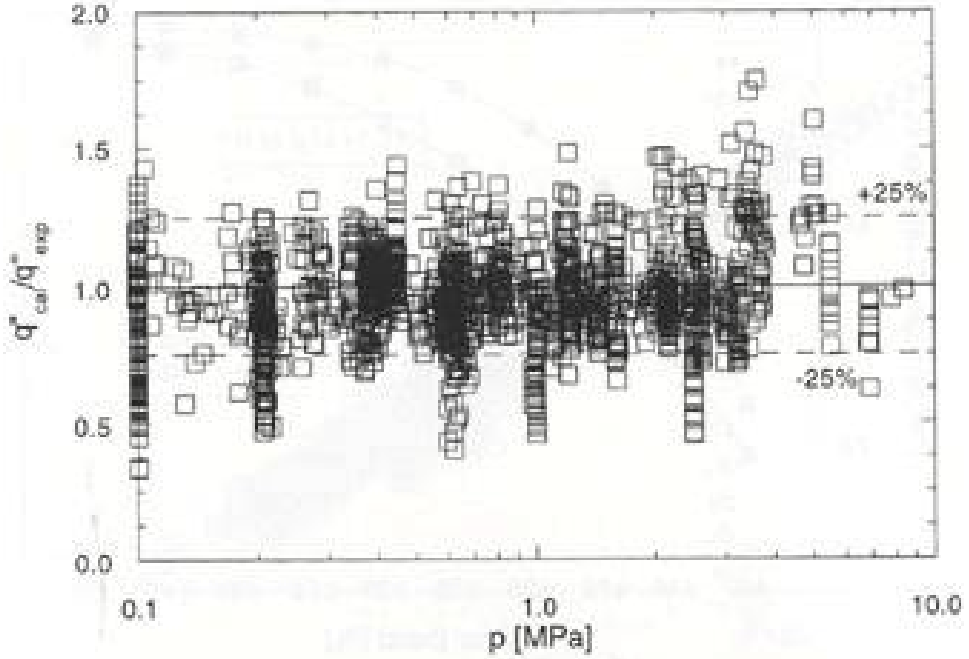

Fig. 16. Ratio of the calculated to the experimental CHF versus pressure.

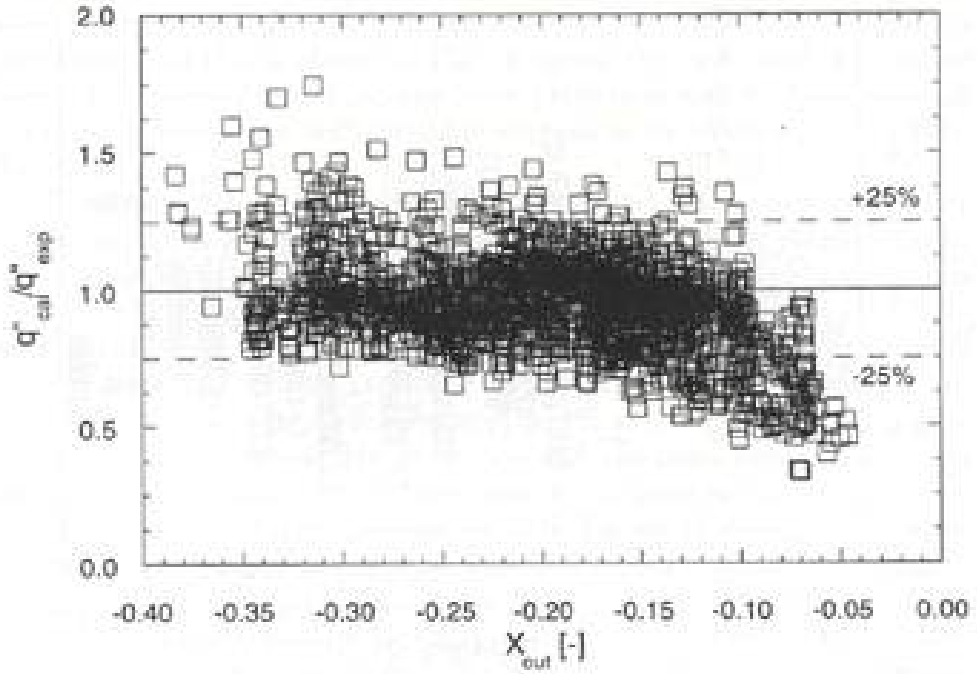

Fig. 17. Ratio of the calculated to the experimental CHF versus exit quality.

the purposes of the present work. No systematic effect of the pressure is observed (Fig. 16), while a significant underprediction of the CHF is shown for few data points with exit conditions close to the saturation (Fig. 17). It is obvious that approaching the saturation conditions, the assumptions made in the construction of the model may not hold any longer, and the model shows a systematic error. Geometric parameters (L/D and D) do not show any systematic influence on the model predictions.

8. Parametric trends of the CHF model

It is of interest to verify the parametric trends of the model for the subcooled CHF. This latter is a function of thermal hydraulic conditions (mass flux, pressure and subcooling) and geometric parameters (channel diameter and length). The parametric trends of subcooled CHF at medium/low pressure, very high mass flux, high and very high subcooling, and small/very small tube diameter, typical of fusion reactor thermal hydraulics, as reviewed by Celata [4], can be summarized as follows:

* CHF increases as mass flux increases.
* CHF is practically independent of the pressure.
* CHF increases with increasing degree of subcooling.
* CHF increases as tube diameter decreases.

Figures 18 through 21 show the calculated and the experimental CHF versus mass flux, pressure, inlet subcooling and exit quality, and tube diameter, respectively, for typical data points selected from the high heat flux data set. Figure 18 shows that the model provides the same observed experimental trend of CHF versus mass flux, for a wide range of G [7]. The negligible dependence of CHF on exit pressure is matched by the model at low pressure [14] and medium pressure [7], as shown in Fig. 19. The almost linear dependence of the CHF on the liquid subcooling is verified in Fig. 20, where the CHF is plotted versus exit quality [61]. The dependence of the CHF on D at small diameters is well predicted by the model, together with the inter-relation between tube inside diameter and liquid velocity as shown in Fig. 21.

The parametric trends shown in Figs. 18-21, demonstrate that the proposed model is very accurate in predicting independent CHF variations with respect to mass flux, pressure, liquid subcooling and channel diameter in the range of high heat fluxes, i.e., high mass flux and high subcooling.

Finally, to give an idea of the order of magnitude of the several parameters involved in the CHF calculation, Fig. 22 shows the normalized data of the predicted CHF, the vapour blanket velocity U_b, the wall temperature T_w, the initial liquid sublayer thickness δ, the length of the vapour blanket L_b, and its equivalent diameter D_b, as a function of mass flux for data reported in [7] (top figure), and as a function of pressure for data reported in [61] (bottom figure).

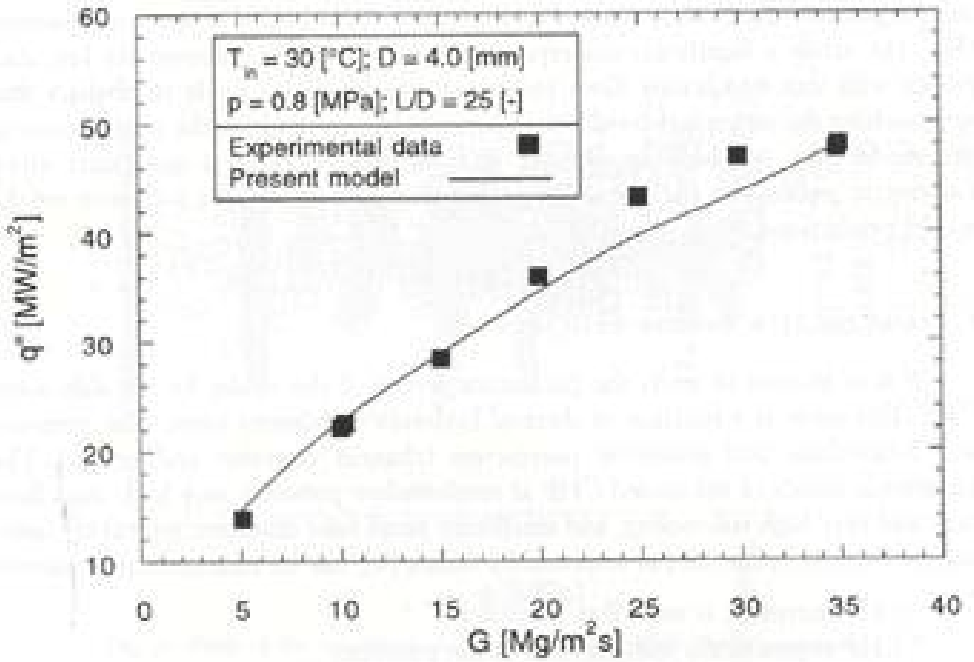

Fig. 18. Mass velocity effect on CHF.

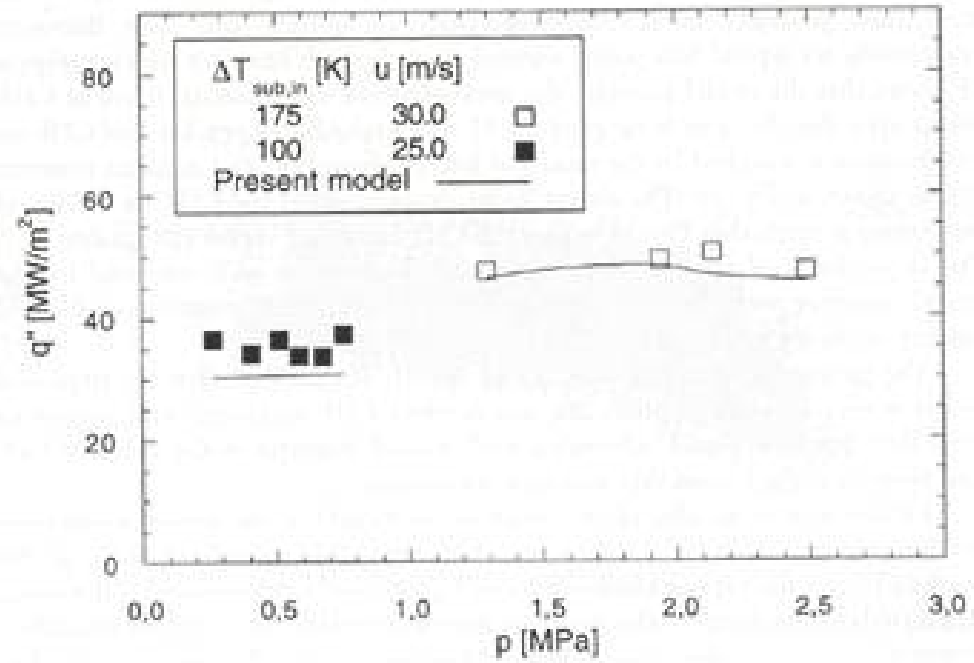

Fig. 19. Pressure effect on CHF.

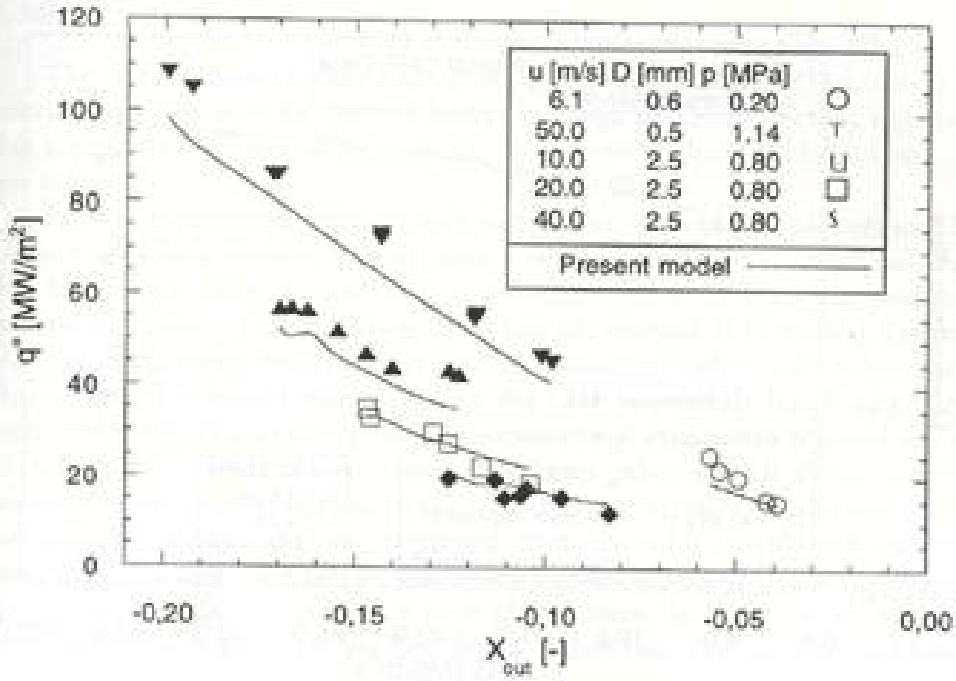

Fig. 20. Exit quality effect on CHF.

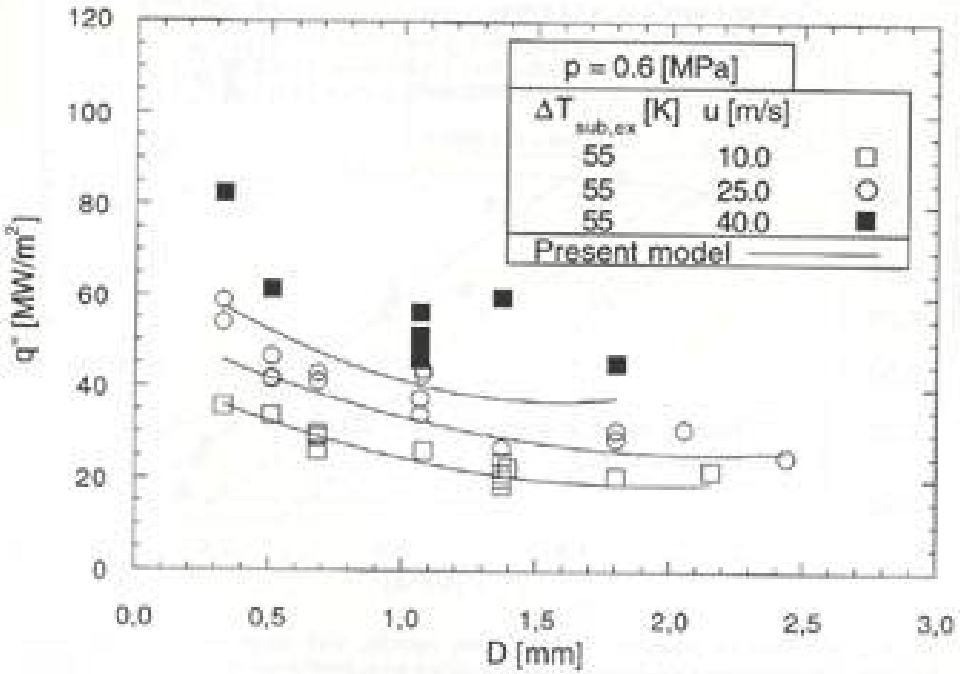

Fig. 21. Diameter effect on CHF.

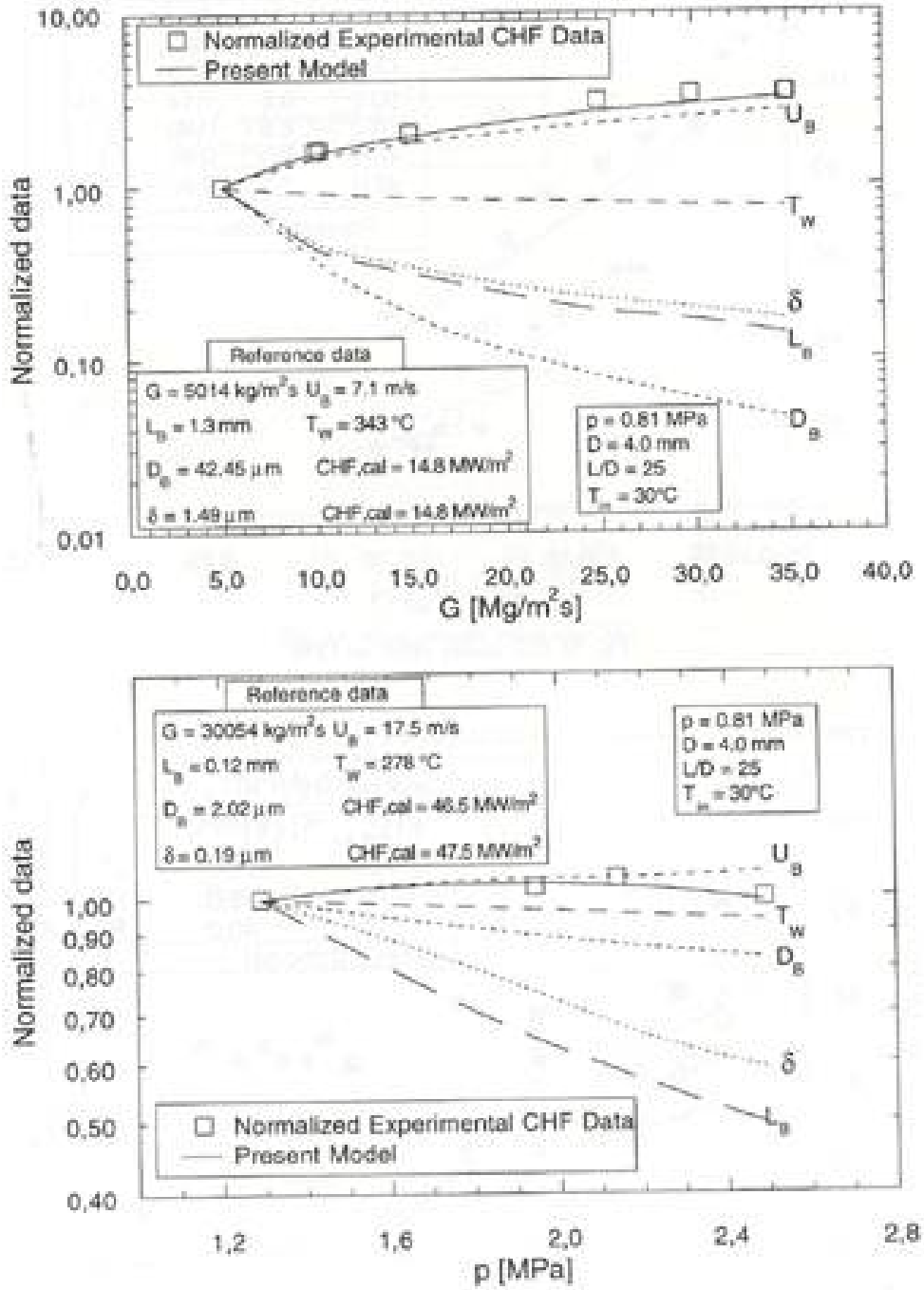

Fig. 22. Typical values of predicted CHF, blanket velocity, wall temperature, initial sublayer thickness, blanket lenght and equivalent diameter, as a function of mass flux [7] (top figure) and pressure [61] (bottom figure).

9. Modelling of peripheral non-uniform heating

The effect of non-uniform heating along the circumference of the tube is of relevant importance in the thermal hydraulic design of fusion reactors high heat flux components. In fact, as an example, the divertor is thermally loaded only on one side.

Ad hoc experiments were recently carried out by Nariai *et al.* [62] and by Gaspari [63]. In particular, Gaspari gave a comparison between peripherally full and half-heated tubes, straight flow, analyzing the CHF at both inlet and exit thermal hydraulic conditions. Using a 10 mm i.d. channel, 0.15 m long, Gaspari observed that, under constant inlet liquid subcooling, higher CHF values were observed for half-heated tubes. Plotting the CHF versus exit liquid subcooling such differences tend to disappear. This experimental evidence is reported in Fig. 23, where the CHF is plotted versus inlet/outlet subcooling. It shows that the influence of the channel heating on the boiling crisis (circumferentially uniform or non-uniform heating) may be neglected once the CHF is referred to local conditions. The latter is a further confirmation that the boiling crisis in subcooled flow boiling can be regarded as a local phenomenon. In Nariai *et al.* the non-uniform heating is such that the heat flux is higher over 180° or 270° and lower

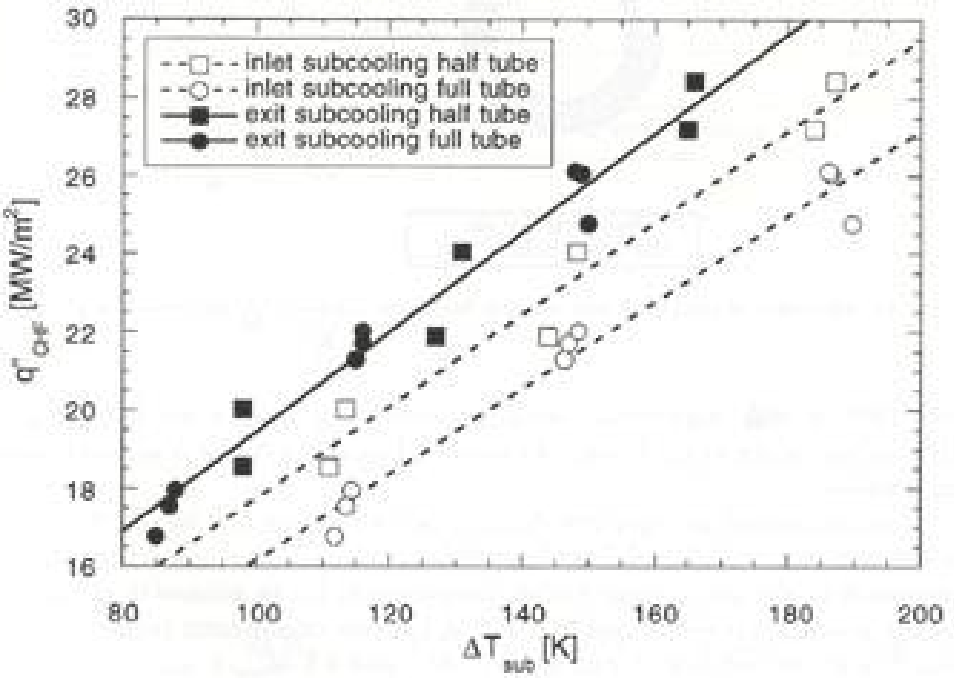

Fig. 23. Influence of peripheral non-uniform heating on CHF. Analysis at local and inlet conditions (Gaspari [63]).

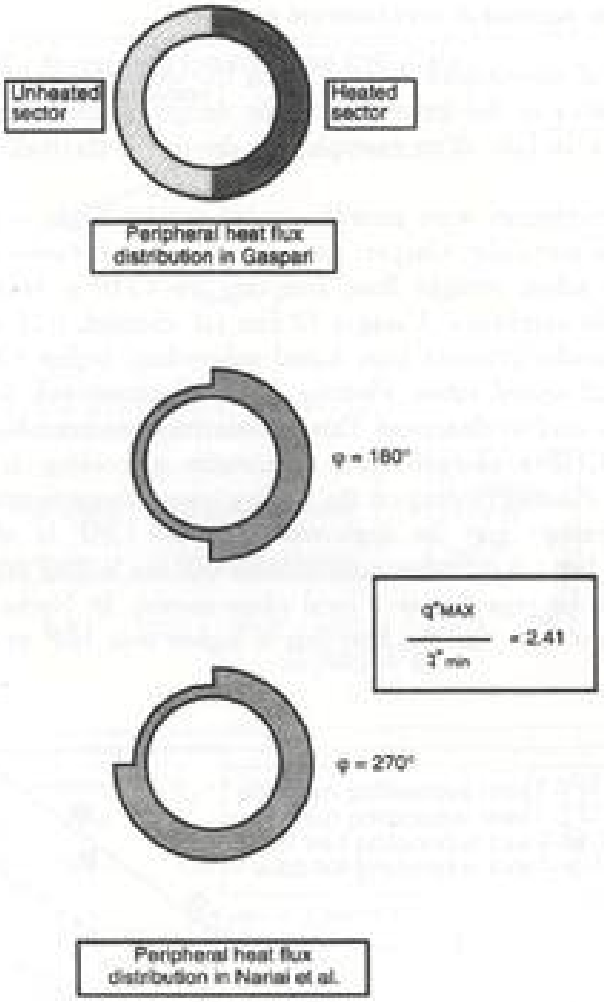

Fig. 24. Schematic of peripheral non-uniform heating in Gaspari [63] and Nariai *et al.* [62].

over 180° or 90°, respectively, being different from zero in the latter regions (thinned part of the tube). Figure 24 shows a schematic of Nariai *et al.* and Gaspari experiments.

Circumferential non-uniform heating can be accounted for in the model description simply by changing the heat flux, q'', in the coolant heat balance for the calculation of the exit average coolant temperature, T_{av}. In particular, we have to use the average heat flux, equal to 0.5 q'' in Gaspari experiments (where q'' is the heat flux in the half-heated part of the tube), and 0.5 $(q''_{max} + q''_{min})$ for $j = 180°$ tests, and 0.75 q''_{max} + 0.25 q''_{min} for $j = 270°$ tests in Nariai *et al.* experiments (where q''_{max} + q''_{min} are the higher and the lower heat flux, respectively). It is evident that

exit bulk thermal hydraulic conditions, which the CHF is strongly dependent on [1], are only a function of the average heat flux (i.e., the total thermal power delivered to the fluid) independent of its distribution.

As boiling crisis in subcooled flow boiling is a strictly local phenomenon, all equations employed in the model mathematical description can be used also in the case of peripheral non-uniform heating. In fact, all calculations, except for T_{in}, are made using the maximum value of the heat flux, and all parameters used to calculate the CHF are local values: d, U_B, L_B, T_w, D_B, y^*. Temperature and velocity distributions are still valid in the sector interested by the heat flux, as in Gaspari experiments, or the highest heat flux, as in Nariai *et al.* experiments. A possible distortion of such distributions are likely to happen in the bulk of the flow, due to turbulent mixing. As velocity and temperature distributions are used locally in the calculation of the CHF (y^* is of the order of magnitude of some tens of micron), it looks reasonable to continue in making use of such distributions also in the case of peripheral non-uniform heating.

The prediction of the few experimental data carried out by Nariai *et al.* using the present model is shown in Fig. 25 where the ratio between the calculated and the experimental critical heat flux is plotted versus the exit quality, x_{out}. The heating non-uniformities investigated. There is a tendency to underestimate the CHF as exit thermal hydraulic conditions approach the bulk saturation ones. The

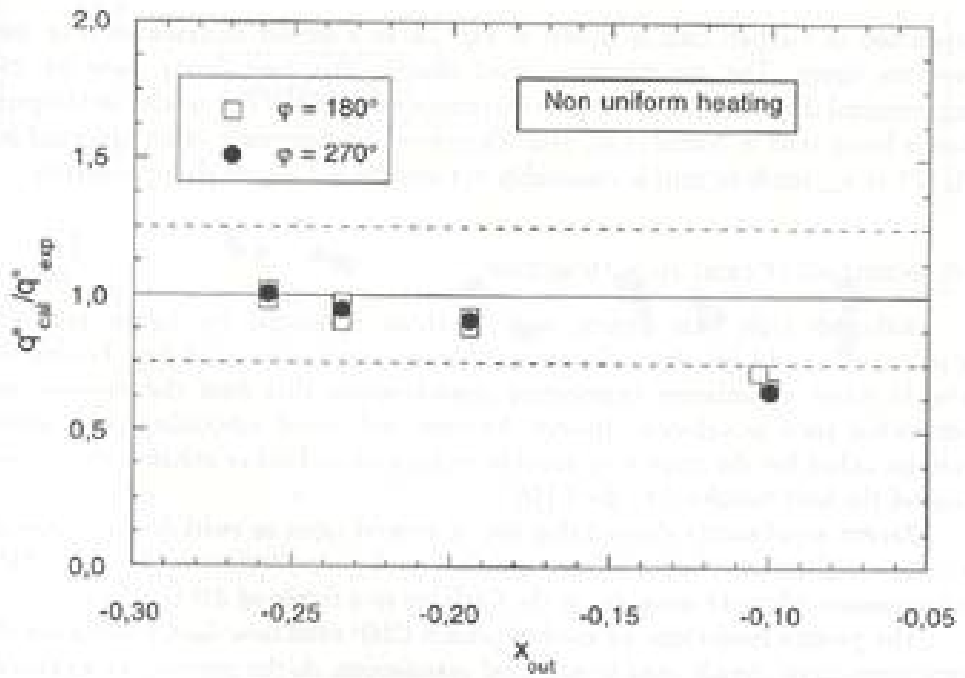

Fig. 25. Prediction of peripheral non-uniform heating, straight flow CHF data [62].

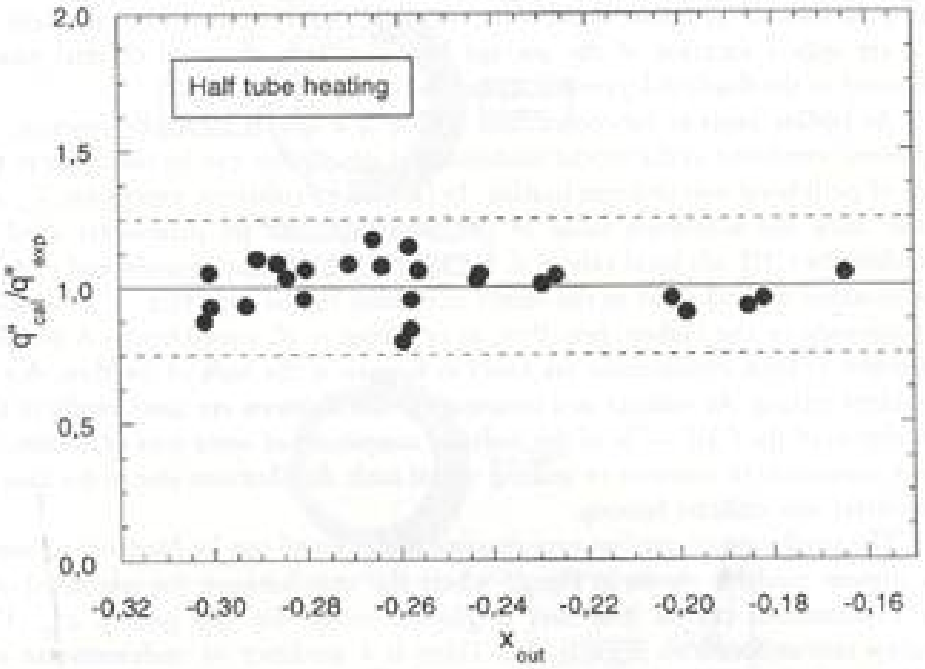

Fig. 26. Prediction of peripheral non-uniform heating, straight flow CHF data [63].

prediction of Gaspari data is shown in Fig. 26, in a similar representation as the previous figure. The agreement is good also in this case, being most of 26 experimental data within ± 20%. The maximum value of the exit quality in Gaspari data is lower than in Nariai *et al.* data. Therefore, the systematic effect observed in Fig. 25 as x_{out} tends to zero is reasonably not evident in Gaspari data prediction.

10. Modelling of swirl flow promoters

Although high heat fluxes, such as those requested for fusion reactors applications, could be physically obtained using water subcooled flow boiling in straight tubes, nonetheless engineering considerations that limit the variation of parameters such as velocity, channel diameter and liquid subcooling, and safety margins called for the employ of suitable techniques to further enhance the upper limit of the heat transfer, i.e., the CHF.

Recent experiments showed that use of twisted tapes as swirl flow promoters in water subcooled flow boiling revealed to be very effective in the CHF enhancement, allowing increases in the CHF up to a factor of 2.0 [29, 64].

The present model may be used to predict CHF swirl flow data, making use of same corrections already used in empirical correlations. As the presence of a twisted tape inside a channel is associated with a relevant increase in the pressure drop (e.g.,

up to a factor of 11 in [64]), a friction factor correction for twisted tapes was suggested by Lopina and Bergles [65]. Based on experiments, Lopina and Bergles show that the friction factor, f_a, for use in the twisted tape geometry varies as:

$$f_a = 2.75\, f\, \gamma^{0.406} \tag{26}$$

where γ is the twist ratio of the tape, a measure of the number of tube diameters per 180° twist in the tape, and f is the friction factor for straight tube. To extend the present model for use with twisted tapes, equation (26) was tried.

The prediction of Nariai *et al.* data [29] is shown in Fig. 27, where the ratio between the calculated and the experimental CHF is plotted versus exit quality, x_{out}. The agreement is quite encouraging as almost all the data are predicted within ± 25%, showing that the procedure can be successful.

Recent experiments by Cardella *et al.* [64] were carried out with twisted tapes inserted in peripherally half-heated tubes. In addition to the above correction for twisted tapes, the model was used as described in section 9. The results of the prediction are shown in Fig. 28, similarly to the previous figure. The agreement can be considered satisfactory in view of the complexity of the situation in comparison with the original description of the model. Although a general underestimation of the CHF is observed, most of the experimental data are predicted within ± 25%.

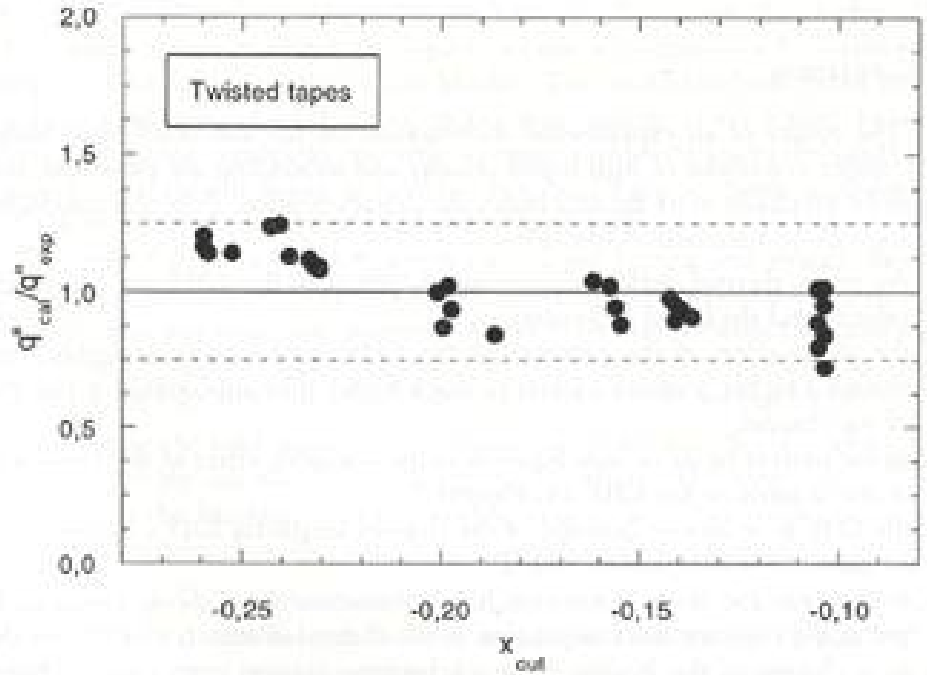

Fig. 27. Prediction of swirl flow CHF data [29].

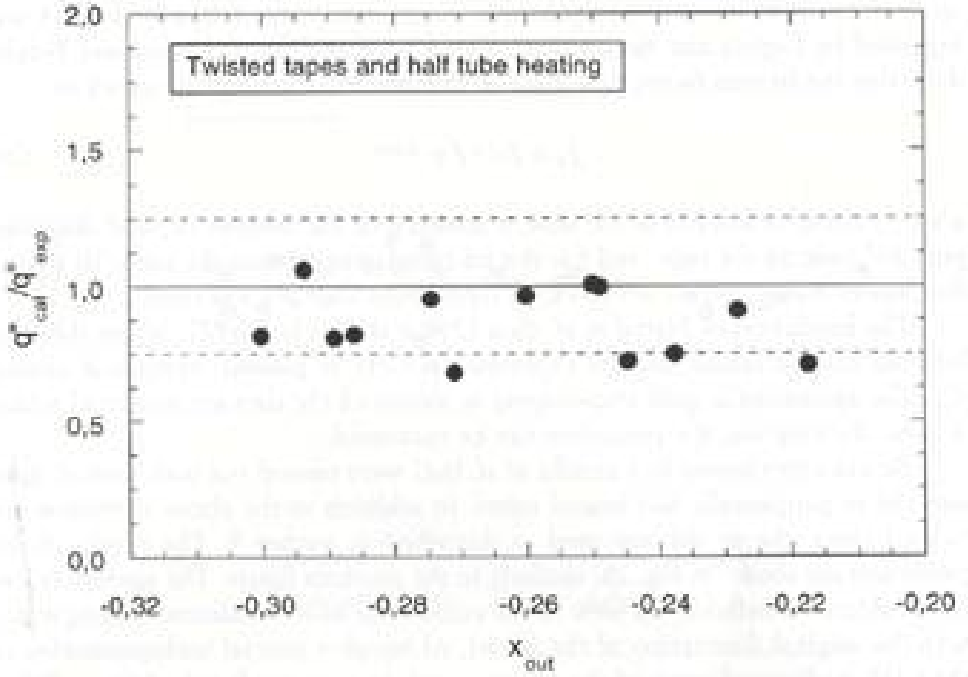

Fig. 28. Prediction of swirl flow, peripheral non-uniform heating CHF data [64].

11. Conclusion

The results of an experimental investigation on the subcooled flow boiling CHF under conditions of high liquid velocity and subcooling are presented, with particular emphasis to its thermal hydraulic characterization. Principal concluding remarks can be summarized as follows:

- the main thermal hydraulic parameters affecting the CHF are the liquid velocity and the liquid subcooling;
- the direct effect of the pressure on the CHF is practically negligible, even though a higher pressure enables to reach higher inlet subcoolings at the inlet of the channel;
- in the present range of high liquid velocity, negligible effect of the orientation of the channel on the CHF was observed;
- the CHF is an inverse function of the channel length for $L/D \leq 30$; for $L/D > 30$ the CHF is independent of L/D;
- this is true for $D \geq 0.7$ mm; for lower diameters the CHF is found to be practically constant and independent of the channel diameter. This may be due to a change in the boiling crisis mechanism, passing from liquid sublayer dryout model (large diameters) to 'flooding' of the channel by the vapour

phase. This latter is due to the size of the bubbles which may be of the same order of magnitude for channel diameter below 0.7 mm.
— Over a large range of tube wall thickness, the CHF is almost independent of the wall thickness, thus homogenizing most of existing experimental data;
— for given values of exit thermal hydraulic conditions, heated length and liquid velocity, the CHF increases with the decrease of tube inside diameter;
— a maximum CHF of about 70 MW/m² was reached with smooth tubes under the following conditions: T_{in} = 0 °C, p = 0.8 MPa, u = 50 m/s, D = 1.2 mm, L = 0.048 m;
— helically coiled wires (d = 1.0 mm, pitch = 20.0 mm) allowed an increase of the CHF up to 50%, with reference to smooth channels, coupled with a moderate increase of pressure drop (25%);
— pressure revealed a negative effect on the relative efficiency of turbulence promoters.

A newly developed model for the prediction of the CHF in water subcooled flow boiling is presented. It is specifically thought to predict the CHF under conditions of high mass flux (G up to 90 Mg/m²s), intermediate-to-low pressure (p < 8.4 MPa), high liquid subcooling (up to 255 K), typical of the thermal hydraulic design of high heat flux components in fusion reactors. The model is based on the observation that, during fully developed boiling, a vapour blanket forms in the vicinity of the heated wall by the coalescence of small bubbles, leaving a thin liquid sublayer in contact with the heated wall beneath the blanket. The CHF is assumed to occur when the liquid sublayer is extinguished by evaporation during the passage time of the vapour blanket. The model has been tested over a very large data bank of CHF in subcooled flow boiling, characterized by wide ranges of operating conditions, showing a general good accuracy in the prediction of experimental data. It looses its validity when local thermodynamic conditions at the CHF approach the saturated state of the liquid bulk.

The model is developed for peripheral uniform heating and straight flow in the channel. Nonetheless, peripheral non-uniform heating is typical of some high heat flux components (i.e., the divertor), as well as the use of twisted tapes as swirl flow promoters for the CHF enhancement is pursued. The model may easily account for the two above situations (also simultaneously occurring) by:

— considering the total thermal power delivered to the fluid in the coolant heat balance for the calculation of local thermal hydraulic conditions;
— modifying the friction factor for straight flow to take into consideration the relevant pressure drop increase due to swirl flow promoters insert.

With the above considerations, the model shows a good capability to predict CHF experimental data carried out with peripheral non-uniform heating and/or swirl flow promoters inserts, resulting a suitable tool for the thermal hydraulic design of fusion reactors high heat flux components.

NOMENCLATURE

C_D	drag coefficient, dimensionless
CHF	critical heat flux, W/m²
C_p	specific heat at constant pressure, J/kg K
D	diameter, m
d	wire diameter, mm
f	friction factor, dimensionless
f(β)	function of contact angle = 0.02-0.03, dimensionless
f_t	twisted-tape friction factor, given by eq. (26), dimensionless
G	mass flux, kg/m²s
g	gravitational acceleration, m/s²
K	thermal conductivity, W/m K
L	length, m
L_e	entrance length, mm
L_b	vapour blanket length, mm
p	pressure, MPa
Pr	Prandtl number: $C_p \mu/K$, dimensionless
Q	group defined in eq. (19)
q''	heat flux, W/m²
R	ideal gas constant on a unit mass basis, radius, m
Re	Reynolds number: GD/μ, dimensionless
S	heat transfer surface, m²
t	wall thickness, mm
T, ΔT	temperature, temperature difference, °C, K
U	velocity, m/s
u	velocity, m/s
U^+	non-dimensional velocity, defined in eqs. (11)-(13)
U_g	vapour blanket velocity, m/s
U_τ	friction velocity: $(\tau_w/\varrho_L)^{0.5}$, m/s
x	steam quality, dimensionless
y	distance from the heated wall, m
y^*	superheated layer, m
y^+	non-dimensional distance from the heated wall, defined in eqs. (11)-(13)

Greek Letters

β	contact angle, dimensionless
δ	liquid sublayer initial thickness, μm
ε	surface roughness, m

Γ	mass flow rate, kg/s
γ	twist tape ratio, the number of tube diameters per 180° twist in the tape, dimensionless also wire pitch, mm
φ	angle, dimensionless
λ	latent heat of vaporization, J/kg
μ	dynamic viscosity, kg/s m
ϱ	density, kg/m^3
σ	surface tension, N/m
τ	passage time of the vapour blanket, s
τ_w	wall shear stress, MPa

Subscripts

B	pertains to the vapour blanket
CHF	pertains to burnout conditions
ex	exit
f	pertains to the liquid in saturated conditions
g	pertains to the vapour
in	inlet
L	pertains to the liquid phase
m	mean
max	maximum
min	minimum
out	exit conditions
sat	pertains to saturated conditions
sub	pertains to subcooled conditions
v	pertains to the vapour phase
w	pertains to the wall

APPENDIX. CHF CALCULATION PROCEDURE

Input parameters G, p_{ex}, D, L, T_{in}.
Assume a value of q''_1. Necessary physical properties are:

C_{pL}, K_L, μ_L, λ, ϱ_L, ϱ_V, σ. Where not specified, physical properties are calculated at saturated state at p_{ex}.

$$T_{in} + \frac{q''S}{\Gamma C_{pL}} = \frac{5}{y^+(R)} T_{m1} + \frac{25}{y^+(R)} T_{m2} + \frac{y^+(R) - 30}{y^+(R)} T_{m3}$$

where C_{pL} is calculated at $(T_m + T_{in})/2$ and T_{m1}, T_{m2} and T_{m3} are calculated from eqs. (22) - (24) using the temperature distributions:

$$T_w - T = QPr\, y^+ \qquad 0 \le y^+ < 5$$

$$T_w - T = 5Q\left\{Pr + ln\left[1 + Pr\left(\frac{y^+}{5} - 1\right)\right]\right\} \qquad 5 \le y^+ < 30$$

$$T_w - T = 5Q\left[Pr + ln\,(1+5Pr) + 0.5\,ln\left(\frac{y^+}{30}\right)\right] \qquad y^+ \ge 30$$

$$Q = \frac{q''}{\varrho_L C_{pL} U_\tau}$$

In the above temperature distribution equations, C_{pL} is calculated at saturated conditions at p_{ex}. From the above calculation T_w is obtained. Using the above temperature distribution equations it is possible to calculate y^+, that is the value of the distance from the heated wall, y, at which the fluid temperature is equal to the saturation value at p_{ex}.

Calculation of D_B:

$$D_B = \frac{32}{f} \frac{\sigma f(\beta)\, \varrho_L}{G^2}$$

where $f(\beta) = 0.03$ and the friction factor f comes from

$$\frac{1}{\sqrt{f}} = 1.14 - 2.0\, log\left(\frac{0.72\, o\varrho_L}{fDG^2} + \frac{9.35}{Re\sqrt{f}}\right)$$

Calculation of δ:

$$\delta = y^* - D_B$$

Calculation of C_D:

$$C_D = \frac{2}{3}\frac{D_B}{\left(\frac{\sigma}{g(\varrho_L - \varrho_V)}\right)^{0.5}}$$

Calculation of U_B and L_B (linked each other):

$$U_B = \left(\frac{2L_B\, g\, (\varrho_L - \varrho_V)}{\varrho_L C_D}\right)^{0.5} + 0.125\,(\delta + \frac{D_B}{2})\,\frac{fG^2}{\varrho_L \mu_L}$$

$$U_B = \left(\frac{2L_B\, g\, (\varrho_L - \varrho_V)}{\varrho_L C_D}\right)^{0.5} + 1.768\,\sqrt{f}\,\frac{G}{\varrho_L}\left\{ln\left[0.354\,\frac{G}{\mu_L}\sqrt{f}\,\left(\delta + \frac{D_B}{2}\right)\right] - 0.61\right\}$$

$$U_B = \left(\frac{2L_B\, g\, (\varrho_L - \varrho_V)}{\varrho_L C_D}\right)^{0.5} + 0.884\,\sqrt{f}\,\frac{G}{\varrho_L}\left\{ln\left[0.354\,\frac{G}{\mu_L}\sqrt{f}\,\left(\delta + \frac{D_B}{2}\right)\right] + 2.2\right\}$$

where L_B is given by

$$L_B = \frac{2\pi\sigma(\varrho_V + \varrho_L)}{\varrho_V\,\varrho_L U_B^2}$$

Calculation of q_2^* from:

$$q^* = \frac{\varrho_L \delta \lambda}{L_B}\,U_B$$

The condition of critical heat flux, CHF, is reached when $q_1^* = q_2^*$.

REFERENCES

[1] A.E., Bergles J.G. Collier, J.M. Delhaye, G.F. Hewitt and F. Mayinger, Two-phase flow and heat transfer in the power and process industries, pp. 226-255, Hemisphere Publishing Corporation, New York, 1981.

[2] J.G. Collier, Convective boiling and condensation, 2nd Edition, McGraw Hill, New York, 1981.

[3] Y.Y. Hsu and R.W. Graham, Transport processes in boiling and two-phase systems, pp. 217-252, American Nuclear Society, 1986.

[4] G.P. Celata, Critical Heat Flux in Water Subcooled Flow Boiling: Experimentation and Modelling, *Proc. 2nd European Thermal-Sciences and 14th UIT National Heat Transfer Conference*, Vol. 1, pp. 27-40, Rome 29-31 May 1996.

[5] R.D. Boyd, Subcooled flow boiling critical heat flux (CHF) and its application to fusion energy components. Part I: A review of fundamentals of CHF and related data base, *Fusion Technology*, **7**, n. 1, pp. 7-30, 1985.

[6] R.D. Boyd, Subcooled flow boiling critical heat flux (CHF) and its application to fusion energy components. Part II: A review of microconvective, experimental, and correlational aspects, *Fusion Technology*, **7**, pp. 31-52, 1985.

[7] G.P. Celata, M. Cumo and A. Mariani, Experimental results on high heat flux burnout in subcooled flow boiling, *Energia Nucleare* **10** (1), 46-57 (1993).

[8] R.D. Boyd, Subcooled water flow boiling experiments under uniform high flux conditions, *Fusion Technology*, **13**, pp. 131-142, 1988.

[9] R.D. Boyd, Subcooled water flow boiling at 1.66 MPa under uniform high heat flux conditions, *ASME Winter Annual Meeting*, S. Francisco, December 10-15, 1989 (HTD - Vol. 119, pp. 9-15).

[10] R.D. Boyd, Subcooled water flow boiling transition and the L/D effect on CHF for a horizontal uniformly heated tube, *Fusion Technology*, **18**, pp. 317-324, 1990.

[11] F. Inasaka and H. Nariai, Critical heat flux of subcooled flow boiling with water, *Proc. NURETH-4*, Vol. 1, pp. 113-120, Karlsruhe, October 10-13, 1989.

[12] H. Nariai, F. Inasaka and T. Shimura, Critical heat flux of subcooled flow boiling in narrow tube, *ASME-JSME Thermal Engineering Joint Conference*, Honolulu, March 22-27, 1987.

[13] A. Achilli, G. Cattadori and G.P. Gaspari, Subcooled burnout in uniformly and non-uniformly heated tubes, *European Two-Phase Flow Group Meeting*, Paper C2, Stockholm, June 1-3, 1992.

[14] C.L. Vandervort, A.E. Bergles and M.K. Jensen, Ultimate limits of boiling heat fluxes, *Proc. Eighth Symposium on Energy Engineering Sciences*, ANL, Argonne, pp. 95-102, May 9-11, 1990.

[15] M. Cumo, Subcooled flow boiling CHF at high liquid velocity, *Proc. 1st European Thermal-Sciences and 3rd UK National Heat Transfer Conference*, Vol. 1, pp. 15-33, Sept. 16-18, 1992.

[16] F. Inasaka and H. Nariai, Evaluation of subcooled critical heat flux correlations for tubes with and without internal twisted tapes, *Proc. NURETH-5*, Salt Lake City, (1992).

[17] S.T. Yin, A. Cardella, A.H. Abdelmessih, Z. Jin and B.P. Bromley, Assessment of a heat transfer correlations package for water-cooled plasma-facing components in fusion reactors, *Proc. NURETH-5*, Salt Lake City, (1992).

[18] J. Weisman and S. Ileslamlou, A phenomenological model for prediction of critical heat flux under highly subcooled conditions, *Fusion Technology* **13**, 654-659 (1988) (Corrigendum in *Fusion Technology* **15**, 1463 (1989).

[19] C.H. Lee and I. Mudawar, A mechanistic critical heat flux model for subcooled flow boiling based on local bulk flow conditions, *Int. J. Multiphase Flow* **14**, 711-728 (1988).

[20] F.C. Gunther, Photographic study of surface-boiling heat transfer to water with forced convection, *Trans. ASME*, 73-2, pp. 115-123, 1951.

[21] G.P. Celata, M. Cumo and A. Mariani, Geometrical effects on the subcooled flow boiling critical heat flux, *European Two-Phase Flow Group Meeting*, Grenoble 2-5 June 1996.

[22] A.E. Bergles, Subcooled burnout in tubes of small diameter, ASME Paper 63-WA-182, 1963.

[23] H. Nariai, and F. Inasaka, Critical heat flux and flow characteristics of subcooled flow boiling with water in narrow tubes, in *Dynamics of Two-Phase Flows*, Jones O.C. and Michiyoshi I. Eds., CRC Press, pp. 689-708, 1992.

[24] W.R. Gambill and J.H. Lienhard, An upper bound for the critical boiling heat flux, *J. Heat Transfer*, **111**, pp. 815-818, 1989.

[25] W.A. Sutherland, Improved heat-transfer performance with boundary-layer turbulence promoters, *Int. J. Heat Mass Transfer*, **10**, pp. 1589-1599, 1967.

[26] P. Kumar and R.L. Judd, Heat transfer with coiled wire turbulence promoters, *The Canadian J. Chemical Engineering*, **48**, pp. 378-383, 1970.

[27] R. Sethumadhavan and M. Raja Rao, Turbulent flow heat transfer and fluid friction in helical-wire-coil-inserted tubes, *Int. J. Heat Mass Transfer*, **26**, n. 12, pp. 1833-1845, 1983.

[28] S.B. Uttarwar and M. Raja Rao, Augmentation of laminar flow heat transfer in tubes by means of wire coil insert, *J. Heat Transfer*, **107**, pp. 930-935, 1985.

[29] H. Nariai, F. Inasaka, W. Fujisaki and H. Ishiguro, Critical heat flux of subcooled flow boiling in tubes with internal twisted tapes, *ANS Winter Meeting*, Session on Fundamentals of Fusion Reactors Thermal-Hydraulics, THD, San Francisco, Nov 11-14, 1991.

[30] W.R. Gambill, R.D. Bundy and R.W. Wansbrough, Heat transfer, burnout and pressure drop for water in swirl flow through tubes with internal twisted tapes, *Chemical Engineering Prog. Symp. Ser. n. 32*, **52**, p. 127, 1961.

[31] G.P. Celata, M. Cumo and A. Mariani, Assessment of correlations and models for the prediction of CHF in subcooled flow boiling, *Energia Nucleare*, **9**, n. 3, 1992.

[32] Y. Katto, A prediction model of subcooled water flow boiling CHF for pressure in the range 0.1-20.0 MPa, *Int. J. Heat Mass Transfer*, **35**, n. 5 pp. 1115-1123, 1992.

[33] L.S. Tong, L.E. Effering and A.A. Bishop, A photographic study of subcooled boiling flow and DNB of Freon-113 in a vertical channel, ASME Paper 66WA/HT-39 (1966).

[34] M.P. Fiori and A.E. Bergles, Model of critical heat flux in subcooled flow boiling, *Proc. 4th Int. Heat Transfer Conf.*, Vol. VI, p. B6.3 (1970).

[35] S.B. van der Molen and F.W.B.M. Galjee, The boiling mechanism during burnout phenomena in subcooled two-phase water flows, *Proc. 6th Int. Heat Transfer Conf.*, Vol. 1, pp. 381-385 (1978).

[36] R. Hino and T. Ueda, Studies on heat transfer and flow characteristics in subcooled flow boiling — Part 2. Flow characteristics, *Int. J. Multiphase Flow* **11**, 283-298 (1985).

[37] R.J. Matteson, F.G. Hammitt and L. S. Tong, A photographic study of the subcooled flow boiling crisis in Freon-113, ASME Paper 73-HT-39 (1973).

[38] L.S. Tong, H.B. Currin, P.S. Larsen and O.G. Smith, Influence of axially nonuniform heat flux on DNB, *Chem. Engng Prog. Symp. Ser.* **62** (64), 35-40 (1965).

[39] S.S. Kutateladze and A.I. Leont'ev, Some applications of the asymptotic theory of the turbulent boundary layer, *Proc. 3rd Int. Heat Transfer Conf.*, Vol. III, pp. 1-6 (1966).

[40] L.S. Tong, Boundary layer analysis of the flow boiling crisis, *Int. J. Heat Mass Transfer* **11**, 1208-1211 (1968).

[41] L.S. Tong, A phenomenological study of critical heat flux, ASME Paper 75-1-1T-68 (1975).

[42] J.C. Purcupile and S.W. Gouse, Jr., Reynolds flux model of critical heat flux in subcooled forced convection boiling, ASME Paper 72-HT-4 (1972).

[43] W.T. Hancox and W.B. Nicoll, On the dependence of the flow-boiling heat transfer crisis on local near-wall conditions, ASME Paper 73-HT-38 (1973).

[44] E.J. Thorgerson, D.H. Knoebel and J.H. Gibbons, A model to predict convective subcooled critical heat flux, *Trans. ASME, Series C, J. Heat Transfer* **96**, 79-82 (1974).

[45] B.R. Bergel'son, Burnout under conditions of subcooled boiling and forced convection, *Thermal Engng* **27**(1), 48-50 (1980).

[46] I.P. Smogalev, Calculation of critical heat fluxes with flow of subcooled water at low velocity, *Thermal Engng* **28** (4), 208-211 (1981).

[47] W. Hebel, W. Detavernier and M. Decreton, A contribution to the hydrodynamics of boiling crisis in a forced flow of water, *Nucl. Engng Des.* **64**, 433-445 (1981).

[48] J. Weisman and B.S. Pei, Prediction of critical heat flux in flow boiling at low qualities, *Int. J. Heat Mass Transfer* **26**, 1463-1477 (1983).

[49] J. Weisman and S.H. Ying, Theoretically based CHF prediction at low qualities and intermediate flows, *Trans. Am. Nucl. Soc.* **45**, 832-833 (1983).

[50] M.A. Styrikovich, E.I. Newstrueva and G.M. Dvorina, The effect of two-phase flow pattern on the nature of heat transfer crisis in boiling, *Proc. 4th Int. Heat Transfer Conf.*, Vol. 9, pp. 360-362 (1970).

[51] R. Mesler, A mechanism supported by extensive experimental evidence to explain high heat fluxes observed during nucleate boiling, *AIChE Journal* **22**, 246-252 (1976).

[52] A.M. Bhat, R. Prakash and J.S. Saini, Heat transfer in nucleate pool boiling at high heat flux, *Int. J. Heat Mass Transfer* **26**, 833-840 (1983).

[53] A. Serizawa, Theoretical prediction of maximum heat flux in power transients, *Int. J. Heat Mass Transfer* **26**, 921-932 (1983).

[54] I.A. Mudawar, T.A. Incropera and F.P. Incropera, Boiling heat transfer and critical heat flux in liquid films falling on vertically-mounted heat sources, *Int. J. Heat Mass Transfer* **30**, 2083-2095 (1987).

[55] Y. Haramura and Y. Katto, A new hydrodynamic model of critical heat flux, applicable widely to both pool and forced convection boiling on submerged bodies in saturated liquids, *Int. J. Heat Mass Transfer* **26**, 389-399 (1983).

[56] T.Z. Harmathy, Velocity of large drops and bubbles in media of infinite and restricted extent, *AIChE Journal* **6**, 281-288 (1960).

[57] M. Ishii and N. Zuber, Drag coefficient and relative velocity in bubbly, droplet or particulate flows, *AIChE Journal* **25**, 843-854 (1979).

[58] F.W. Staub, The void fraction in subcooled boiling - Prediction of the initial point of net vapour generation, *J. Heat Transfer* **90**, 151-157 (1968).

[59] S. Levy, Forced convection subcooled boiling - Prediction of vapour volumetric fraction, *Int. J. Heat Mass Transfer* **10**, 951-965 (1967).

[60] R.C. Martinelli, Heat transfer to molten metals, *Trans. ASME* **69**, 947-951 (1947).

[61] G.P. Celata, and A. Mariani, A Data Set of Critical Heat Flux in Water Subcooled Flow Boiling, *presented at the 3rd Specialists' Workshop on the Thermal-Hydraulics of High Heat Flux Components in Fusion Reactors*, J. Schlosser Ed., Cadarache. (1993)

[62] H. Nariai, F. Inasaka, A. Ishikawa and W. Fujisaki, Critical heat flux of subcooled flow boiling in tube with internal twisted tape under non-uniform heating conditions, *Proc. 2nd JSME-KSME Thermal Engineering Conference*, Vol. 3, pp. 283-288 (1992).

[63] G.P. Gaspari, Comparison among data of electrically and e-beam heated tubes, *Proc. 3rd International Workshop on High Heat Flux Components Thermal Hydraulics in Fusion Reactors*, Cadarache (1993).

[64] A. Cardella, G.P. Celata, G. Dell'Orco, G. Gaspari, G. Cattadori and A. Mariani, Thermal hydraulics experiments for the NET divertor, *Proc. 17th Symposium on Fusion Technology*, Vol. 1, pp. 206-210 (1992).

[65] R.F. Lopina and A.E. Bergles, Heat transfer and pressure drop in tape-generated swirl flow of single-phase water, *J. Heat Transfer* **91**, 8-13 (1969).